Somatic mutations reveal hyperactive Notch signaling and racial disparities in prurigo nodularis

Ahmad Rajeh[1], Hannah L. Cornman[1], Anuj Gupta[2], Mindy D. Szeto[1], Anusha Kambala[1], Olusola Oladipo[1], Varsha Parthasarathy[1], Junwen Deng[1], Sarah Wheelan[3], Thomas Pritchard[1], Madan M. Kwatra[4], Yevgeniy R. Semenov[5,6], Alexander Gusev[7,8], Srinivasan Yegnasubramanian[2,9], Shawn G. Kwatra[1,9]

[1]Department of Dermatology, Johns Hopkins University School of Medicine, Baltimore, MD, USA.
[2]The Sidney Kimmel Comprehensive Cancer Center, Baltimore, MD, USA.
[3]Present affiliation: National Human Genome Research Institute, National Institute of Health, Bethesda, MD, USA.
[4]Department of Anesthesiology, Duke University School of Medicine, Durham, NC, USA.
[5]Department of Dermatology, Massachusetts General Hospital, Boston, MA, USA.
[6]Department of Systems Biology, Harvard Medical School, Boston, MA, USA.
[7]Division of Genetics, Brigham & Women's Hospital, Boston, MA, USA.
[8]Department of Medical Oncology, Dana-Farber Cancer Institute, Boston, MA, USA.
[9]Department of Oncology, Johns Hopkins University School of Medicine, Baltimore, MD, USA.

Corresponding author:

Shawn G. Kwatra, MD
Associate Professor of Dermatology and Oncology
Director, Johns Hopkins Itch Center
Johns Hopkins University School of Medicine
Office: Room 206, Lab: Suite 216, Koch CRBII
1550 Orleans Street, Baltimore, MD 21231, USA
Tel: 410-955-8662
Email: skwatra1@jhmi.edu

Conflict-of-interest statement

S.G.K. is an advisory board member/consultant for Abbvie, Aslan Pharmaceuticals, Arcutis Biotherapeutics, Celldex Therapeutics, Galderma, Genzada Pharmaceuticals, Incyte Corporation, Johnson & Johnson, Novartis Pharmaceuticals Corporation, Pfizer, Regeneron Pharmaceuticals, and Sanofi and has served as an investigator for Galderma, Pfizer, Incyte, and Sanofi. S.Y. receives research funding to his institution from Bristol-Myers Squibb and Celgene, Janssen, and Cepheid for unrelated work and has served as a consultant for Cepheid. He owns founder's equity in Brahm Astra Therapeutics and Digital Harmonic. All other authors declare they have no competing interests.

Abstract

Prurigo nodularis (PN) is a chronic inflammatory skin disease that disproportionately affects African Americans and is characterized by pruritic skin nodules of unknown etiology. Little is known about genetic alterations in PN pathogenesis, especially relating to somatic events which are often implicated in inflammatory conditions. We thus performed whole-exome sequencing on 54 lesional and nonlesional skin biopsies from 17 PN patients and 10 atopic dermatitis (AD) patients for comparison. Somatic mutational analysis revealed that PN lesional skin harbors pervasive somatic mutations in fibrotic, neurotropic, and cancer-associated genes. Nonsynonymous mutations were most frequent in *NOTCH1* and the Notch signaling pathway, a regulator of cellular proliferation and tissue fibrosis, and *NOTCH1* mutations were absent in AD. Somatic copy-number analysis, combined with expression data, showed that recurrently deleted and downregulated genes in PN lesional skin are associated with axonal guidance and extension. Follow-up immunofluorescence validation demonstrated increased *NOTCH1* expression in PN lesional skin fibroblasts and increased Notch signaling in PN lesional dermis. Finally, multi-center data revealed a significantly increased risk of *NOTCH1*-associated diseases in PN patients. In characterizing the somatic landscape of PN, we uncover novel insights into its pathophysiology and identify a role for dysregulated Notch signaling in PN.

Introduction

Prurigo nodularis (PN) is a chronic inflammatory skin disease characterized by intensely pruritic, hyperkeratotic skin nodules on the trunk and extremities (1, 2). Compared to more common and better characterized chronic pruritic dermatoses like atopic dermatitis (AD) or psoriasis, PN is associated with greater itch intensity (3), as well as a significant quality of life impairment (4, 5). PN emerges in middle age, disproportionately affects African Americans, and is associated with multiple systemic conditions (6–9). Despite this significant clinical burden, the etiology of PN remains poorly understood.

The current understanding of PN biology centers around an interplay between cutaneous inflammation, neuronal dysregulation, and altered keratinocyte differentiation and fibroblast signaling (10–13). Recent transcriptomic studies show characteristic patterns of immune polarization in PN patients, including both Th2/Th17-centered cutaneous immune activation, and cutaneous and systemic Th22-related cytokine upregulation (10, 14). Black patients have a greater genetic risk of developing PN and distinct inflammatory signatures are seen in African American PN patients, suggesting the existence of multiple disease endotypes (15–17). However, to which extent those patterns might be explained by genetic variation or environmental exposures remains unknown. In better studied chronic pruritic dermatoses such as AD and psoriasis, genomic studies have accelerated our understanding of disease pathology and informed new treatments (18, 19), but similar investigations are lacking for PN.

The relevance of genomic studies in inflammatory skin disease includes postzygotic variation. Somatic mutations throughout the body are known to drive neoplasms, but growing evidence also points to clonal expansions harboring somatic mutations in non-neoplastic disease and healthy-appearing tissue, including the skin (20–23). Such findings have informed our understanding of both the disease and the corresponding tissue biology. For example, colonic mucosa of patients with inflammatory bowel disease displays positive selection for

mutations in interleukin-17 pathway genes, which may confer a protective advantage to mucosal epithelia (20, 24). Thus, delineating somatic events associated with PN may further our understanding of not only disease pathology, but also cutaneous molecular adaptations in the setting of chronic itch, fibrosis, and neuroinflammation. This is especially pressing given the comorbidities in PN patients, including a higher risk of skin and internal malignancies (25, 26), which remain largely unexplained.

In this study, we characterize the landscape of somatic events in PN lesional skin. We perform whole-exome sequencing (WES) on individual-matched lesional and nonlesional skin biopsies from a diverse cohort of PN patients, as well as AD patients as a reference group. We explore the mutational landscape of PN at the individual nodule level, identifying somatic events in lesional PN skin compared to adjacent healthy-appearing skin. We also contrast the somatic profile of PN to that of AD to elucidate molecular pathways specific to PN. Our somatic analysis also leads us to functional and multi-center epidemiological follow-up investigations. To our knowledge, this work represents the first and largest genomic study of PN.

Results

Whole-exome analysis

An illustration of the study design is shown (Figure 1A). Briefly, we recruited 17 patients from the Johns Hopkins Itch Center diagnosed with PN (Figure 1B and C) fulfilling our selection criteria (see Methods). Patient demographics are summarized in Figure 1D. Two skin punch-biopsies were obtained from each patient, one from a prurigo nodule (lesional) and one from normal-appearing skin (nonlesional) within 10 cm of the nodule. Since high-throughput WES can provide sufficient resolution for the detection of somatic events, we generated WES data from 17 lesional and 17 nonlesional PN samples in this study. In the same method, we also

generated 20 matched WES datasets from 10 patients with AD for use as reference group (Figure 1A and D).

From our PN cohort (34 WES datasets across 17 patients), we obtained approximately 1.7 billion reads (mean and range = 4.9×10^7 [4.2×10^7 to 6.1×10^7] and 5.2×10^7 [4.3×10^7 to 7.0×10^7] for lesional and nonlesional samples, respectively). After quality control and alignment to the hg38 human reference genome, we noted an average sequencing coverage of 195 (187 and 202 for lesional and nonlesional, respectively). On average, more than 93% of the exome was sequenced to at least 20X depth, providing a reliable signal for variant calling (27). Detailed sequencing and alignment information, including results from preprocessing and variant calling on our AD control cohort, is provided (Table S1). One pair of AD lesional/nonlesional samples was excluded from downstream analyses because the nonlesional sample had less than 50% of the exome sequenced to at least 20X depth.

Somatic variation in PN lesional skin

Somatic variants in PN nodules were identified by matching PN lesional to nonlesional samples per patient. The landscape of somatic mutations in PN is shown in Figure 1E-H. Following quality control, we identified 2387 high-confidence somatic single nucleotide variations (SNVs) SNVs and small insertions/deletions (indels) in PN lesional skin affecting 1933 genes. Mutational analysis showed a median of 75 somatic (lesion-specific) mutations per patient, including SNVs and indels. We observed a median mutational burden of approximately 0.52 per megabase of coding region (range of 0.26 to 9 per megabase; outlier sample was further characterized in Figure S1). We noted 35% (847 of 2387), 2.0% (48 of 2387), 0.59% (14 of 2387), 0.58% (13 of 2387), and 0.3% (8 of 2387) missense, nonsense, splice site altering, in-frame indels, and frameshift indels, respectively. After predicting the effects of variants on protein function, variants were classified into significance categories “High + Moderate”, indicating likely change in protein sequence, and “Low + Modifier”, indicating no known change

in protein sequence (Figure 1F). We found a median of 29 functional, lesion-specific somatic SNVs or indels per PN patient (range of 13 to 450) (Figure 1F).

We observed a median somatic variant allele frequency (VAF) of 0.031 (range of 0.01 to 0.449) in PN lesional skin, with Caucasian PN patients displaying a higher VAF than African American PN patients (0.033 compared to 0.029, $P = 0.0056$, *Wilcoxon*) (Figure 1G and H). On assessment of somatic variants at the gene level, there were 46 genes with nonsynonymous somatic mutations in at least two out of 17 patients with PN. We grouped recurrently-mutated genes using three *a priori*-defined gene sets relevant to PN based on literature and clinical judgement. There were 5 genes associated with pathologic fibrosis (*NOTCH1*, *SCN5A*, *MAP1B, TTN*, *ITPR1*) (28), 6 genes associated with neuronal migration or projection (*MAP1B*, *RELN*, *TENM1*, *CNTN2, NAV1, RGS12*) by gene ontology, and 4 cancer-associated genes (*NOTCH1*, *TRRAP, FAT1*, *NCOA1*) according to the Cancer Gene Census (CGC) from the Catalogue of Somatic Mutations in Cancer (COSMIC) (29). *NOTCH1* had the most frequent nonsynonymous somatic mutations: we found 4 missense SNVs (p.Arg1962His, p.Asn70Ile, p.Glu450Lys, and p.Asn325Lys) and 1 in-frame deletion (p.Val413-Asp414del) across 4 patients, 2 of whom were African American. *NOTCH1* is an intracellular regulator of the Notch family with pleiotropic functions in cellular proliferation and tissue fibrosis, and a known hallmark driver of cutaneous squamous cell carcinoma (cSCC) (30, 31). 3 out of 5 identified *NOTCH1* mutations where within the extracellular epidermal growth factor (EGF)-like domain, which is involved in ligand binding and preventing constitutional activation (32). Somatic mutations in *NOTCH1* had a significant co-occurrence with mutations in *NCOA1, MISP*, *NAV1*, *MYO1C*, *RGS12*, and *VPS13B* ($P < 0.05$, pairwise *Fisher's exact test*) (Figure 2A).

Genes associated with fibrosis. In addition to *NOTCH1*, we identified somatic mutations in other profibrotic genes. We noted two missense mutations in *SCN5A* (p.Gly1158Asp, p.Arg1638Gln) across two PN patients. *SCN5A* encodes the alpha subunit of the $Na_v1.5$ sodium

channel, which plays a key role in the depolarization of cardiomyocytes and whose channelopathy is linked to cardiac fibrosis (33). *SCN10A* from the same gene family, which encodes $Na_v1.8$, which regulates pro-inflammatory responses in the skin and was significantly upregulated in the epidermis of rosacea and psoriasis skin lesions (34).

We found two missense mutations in *ITPR1* (p.Ala805Val, p.Glu914Lys) affecting two PN patients. *ITPR1* encodes one of the three members of the IP_3-receptor family that form calcium release channels and is associated with pancreatic fibrosis (28), in addition to chronic itch mediated by astrocytes (35). We also observed two recurrent missense mutations in *MAP1B* (p.Val1549Gly x 2) across two patients. While *MAP1B* is thought to be primarily involved in microtubule assembly and neurogenesis, it also plays a role in fibrosis, particularly in the eye (28, 36).

In addition, we found *TTN* mutated in 3 patients including 4 missense mutations (p.Ala25524Val, p.Asn8023Lys, p.Ala35193Thr, and p.Val7022Ala) and one frame-shift deletion (p.Val29546AsnfsTer3). *TTN* has an established role in interstitial fibrosis and is frequently mutated in numerous cancers, but it encodes the largest protein in humans and is frequently mutated in reference populations (37, 38). Of note, we found a recurrent p.Ile1690Val missense mutation in Epiplakin 1 (*EPPK1*) in 3 of the PN patients. While *EPPK1* was not in our pre-defined gene sets, this was the only gene with 3 or more identical recurrent somatic mutations, at either the DNA or amino acid level. *EPPK1* encodes a member of the plakin family which is involved in the organization of cytoskeletal architecture and has been shown to accelerate keratinocyte migration during wound healing (39, 40). We also found several mutations in genes related to neuronal migration or projection, detailed below.

Neurotropic genes. The mutations in *MAP1B* are described above since it is found to have both fibrotic as well as neurotropic functions (28, 36). *RELN*, which is involved in nerve migration, projection, and synaptic plasticity was found to have two missense mutations

(p.Thr468Pro, p.Val167Leu) across two patients. We also found two missense mutations across two patients in *TENM1* (p.Ala2661Ser, p.Gly1134Arg) and *CNTN2* (p.Ala2661Ser, p.Gly1134Arg). *TENM1* encodes a protein of the teneurin subfamily which is thought to function as a neuronal cellular signal transducer and is one of the most highly mutated genes in melanoma (41). *CNTN2* encodes contactin 2, which is found to play an important role in neuronal excitability (42). In addition, we noted two missense mutations across two patients in *RGS12* (p.Gly454Asp, p.Arg403Cys) and *NAV1* (p.Pro1507Ser, p.Arg1581Cys). *RGS12* was shown to be a critical modulator of serotonergic neurotransmission (43), while *NAV1* is a relatively understudied gene that is involved in neuronal development and regeneration (44).

Cancer-associated genes. To identify mutations in known cancer genes, we overlapped our set of 46 genes with recurrent nonsynonymous mutations and the curated CGC gene list from COSMIC (29). We found recurrent mutations in known cancer genes *TRRAP*, *FAT1, and NCOA1*. We found 3 missense mutations in *TRRAP* (p.Pro252Ser, p.Pro1364Leu, p.Glu2479Lys) across two patients. *TRRAP* is involved a cell-cycle regulation and oncogenesis and has been found to be recurrently mutated in melanoma (45, 46). Notably, previous work showed that skin fibroblasts of individuals with *TRRAP* mutations have significant changes in expression of genes associated with neuronal function and ion transport (45). *FAT1*, a regulator of cell-cell adhesion and extracellular matrix architectural integrity that is a recognized driver of cSCC (47), had one nonsense p.Gln2076Ter mutation and one splice site mutation across two patients. We also found two missense mutations in *NCOA1* (p.Pro1102Ser, p.Ala498Thr) across two PN patients.

We further investigated the mutation rate in known oncogenic pathways as reported by The Cancer Genome Atlas (48). We found the Notch signaling pathway to be most commonly mutated in our PN cohort, with variants detected in 9 out of 17 patients (52.9%), including mutations in *NOTCH1, NOTCH4, CNTN6, FBXW7, JAG2,* and *SPEN*. Notch signaling is

followed by the RTK-RAS and Wnt pathways, which were altered in 5 (29.4%) and 4 (23.5%) PN patients, respectively. A list of high-confidence somatic SNV and indel calls made in this study is included in Table S2.

Gene set enrichment analysis. Gene set enrichment analysis offers a relatively unbiased view into the somatic landscape at the pathway level and can highlight patterns that are too subtle to identify at the gene level (49). As a proxy for the somatic selection, we first conducted an enrichment analysis of high-VAF (>0.3) nonsynonymous somatic mutations. Different patterns by race were observed (Figure 2). Notably, high-VAF mutations in African American PN patients were associated with epithelial-to-mesenchymal transition (*NOTCH4* and *TASOR*; FDR-adjusted $P < 0.05$).

We then performed enrichment analysis of all genes that were found to have recurrent nonsynonymous somatic mutations in PN lesions. We included pathways from 3 term databases: Gene Ontology (GO) Biological Process, GO Cellular Component, and NCI-Nature Pathways. After correction for multiple hypothesis testing, the most significantly mutated networks were related to Notch-mediated signaling, neuronal migration, and polymeric cytoskeletal fiber (Figure2, B-D).

Since we identified *NOTCH1* as the most frequently mutated gene in PN lesional skin, and loss-of-function mutations in *NOTCH1* have been established to occur commonly in cSCC (50), we compared our PN somatic calls to a publicly available cSCC variant dataset from a recent metanalysis by Chang et al. (47). We included 83 cSCC samples for this analysis, with a median tumor mutational burden and VAF of 21.4 per megabase and 0.258, respectively. Not surprisingly, cSCC samples had a significantly higher mutational burden and VAF than our PN samples ($P < 0.001$, *Wilcoxon*) (Figure 3A and B). *NOTCH1* was mutated in 55.4% of cSCC samples, second only to *TTN*. Overall, there were 6 genes that mutated in 25% or more of the cSCC samples and also in two or more samples of our PN cohort: *NOTCH1*, *FAT1*, *TTN*, *FLG*,

and *RELN* (Figure 3C-E). Out of those genes, *NOTCH1* and *FAT1*, are the ones previously identified as likely cSCC drivers (47) (Figure 3C-E). In addition, *TASOR2,* a gene found to be differentially regulated in several cancers but whose function remains understudied (51), was the only gene not mutated in any of the cSCC samples while having somatic mutations in two of our PN patients.

Somatic copy number variation in PN

In addition to somatic SNVs and indels, somatic copy-number variation (CNV) may contribute to the phenotype of PN phenotype by altering gene dosage. Copy number analysis of exome data identified a median of 66 somatic CNVs per PN patient (range of 48 to 344), including characteristic recurrent deletions in chromosome 1p13 (6/17; 35%), 4p (5/17; 29%), 4q13.2 (4/17; 24%), 5q (3/17; 18%), 7q21 (3/17; 18%), 11q14 (5/17; 29%), 12 (7/17; 41%), and 19q13.42 (4/17; 24%). Since the method we used gives a greater weight to high amplitude events that are less likely to occur by chance, we also identified significant gains in chromosome 7p22 and chromosome 17q25.3 in one sample ($P < 0.05$; see Methods). We noted distinct patterns of recurrent somatic CNV in PN by race: Caucasian patients more commonly had deletions in chromosome 1p13.3 (4/5; 80%) and duplications in chromosome 15 (3/5; 60%), whereas African American patients more commonly had deletions involving chromosome 4p (5/12; 42%), 4q13.2 (4/12; 33%), 7q21 (3/12; 25%), 11q14 (5/12; 42%), and 12 (5/12; 42%) (Figure 4A-C). Overall, recurrent somatic deletions had an overlap with 3173 gene loci and somatic duplications overlapped with 5 gene loci: *FOXK2*, *WDR45B*, *EIF3B, RSPH10B2*, and *CCZ1B*.

Previous studies show that CNV affects gene expression and biological processes (52, 53). To investigate the functional impact of somatic CNV in PN, we overlapped genes affected by recurrent somatic CNV calls in our PN cohort with genes found to be differentially expressed in PN lesional skin using RNA-seq data (10). We identified 264 genes that were significantly

downregulated (FDR-adjusted $P < 0.05$; log fold-change < 0) as well as recurrently deleted in PN lesional skin. Enrichment analysis of those 264 genes showed that the deleteriously affected pathways were most significantly related to neural crest cell development, negative regulation of chemotaxis, and negative regulation of axonal extension (Figure 4E). Manual review of the enrichment results revealed that it was primarily driven by a recurrent 7q21 deletion affecting *SEMA3C, SEMA3E, SEMA3A,* and *SEMA3D* (Figure 4D). There were two gene loci that overlapped recurrently duplicated segments and were significantly upregulated in PN lesional skin: *FOXK2* and *EIF3B*.

Since not all of the RNA-seq samples we used overlapped with the WES samples, and to demonstrate that the enrichment in neurotropic pathways is driven by somatic deletions, we repeated the enrichment analysis using expression data only as a negative comparator–there was no significant enrichment in those neuronal pathways without CNV information (Figure S2).

We then performed CNV signature analysis to investigate the common etiology, if any, of such wide-scale somatic events. We identified 3 CNV signatures in our samples based on loss-of-heterozygosity status, total copy number state, and segment length. One CNV signature was highly similar to known signature CN12 from the COSMIC curated database (0.837 cosine similarity), which is believed to be a focal loss-of-heterozygosity signature indicating chromosomal instability in association with a enome doubling event (54). African American and Caucasian patients displayed similar exposure to CN12 ($P = 0.58$, *Fisher's exact test*) (Figure 4F-G).

Somatic mutational landscape of PN compared to AD

Distinct somatic mutational landscape in PN. Somatic mutational analysis of AD lesional skin revealed a median of 75 lesion-specific mutations per patient (range of 37 to 1161), with the highest frequency of recurrent nonsynonymous somatic mutations in *TTN* (4/9; 44%), *DNHD1* (3/9; 33%), *USP20* (3/9; 33%), and *ANKRD36* (3/9; 33%) (Figure 5 A). Of note, none of

the AD samples had somatic mutations in *NOTCH1* (Figure 5D). Somatic mutations in AD lesional skin had a median mutational burden of 0.66 per megabase (range of 0.28 to 92.7) and median VAF of 0.04 (range of 0.010 to 0.405), which were significantly higher than those of PN ($P < 0.001$, *Wilcoxon*) (Figure 5B and E).

To investigate the somatic mutational landscape more characteristic of PN compared to AD, we started with the set of 46 genes that had nonsynonymous mutations in at least two PN patients and filtered those genes that had any nonsynonymous mutations in our AD cohort. This analysis yielded 21 genes for PN. We performed enrichment analysis on the resulting gene list. The most significant pathways were related to the Notch-mediated HES/HEY network, E2F transcription factor network, microtubule cytoskeleton, neuron migration, and others (Figure 5F and G).

We found a nonsense mutation (p.Trp1374Ter) and two missense mutations (p.Glu1017Gly, p.Ser1067Leu) across two AD patients in *DUOX2*. Notably, the same nonsense mutation in *DUOX2* appeared in one PN sample and this is the only recurrent nonsense mutation we observed across both conditions. *DUOX2* is primarily responsible for the release of hydrogen peroxide through NADPH oxidase and variant protein products have been associated with elevated plasma IL17C levels (55, 56).

Mutational signatures. Analysis of the mutational processes in PN and AD lesional skin identified the presence of 4 single-nucleotide substitution (SBS) and 2 double-nucleotide substitution signatures (DBS). SBS signatures were most similar to SBS7b (UV exposure; similarity: 0.966), SBS6 (DNA mismatch repair; similarity: 0.806), and SBS5 (unknown etiology, similarity: 0.781), from the COSMIC database (57) (Figure 5A). SBS5 has unknown etiology but it is found to have increased burden in many cancer types and is clock-like in that its exposure correlates with the age of the individual (57). We also detected a de-novo SBS signature in AD and PN characterized by frequent A[T>]G and G[C>T]C substitutions. SBS signatures had

similar distribution across PN and AD groups. DBS signatures only correlated with DBS1 (UV exposure; similarity: 0.999), characterized by transcriptional bias with more CC>TT substitutions. We also identified a de-novo DBS signature characterized by frequent TG>CA substitutions. For each detected mutational signature, a multiple linear regression model was built to test if age, sex, PN diagnosis (compared to AD diagnosis), and itch intensity significantly predicted the corresponding signature's exposure. The regression model of DBS1 was statistically significant (goodness-of-fit adjusted $R^2 = 0.66$, $P = 0.004$). DBS1 was significantly associated with PN diagnosis ($\beta = 0.779$, $P < 0.001$) and itch intensity ($\beta = 0.187$, $P = 0.003$).

Immunofluorescence analysis. Our somatic analyses identified *NOTCH1* as the most frequently mutated gene in PN lesional skin. As functional validation, we performed immunofluorescent (IF) staining of four lesional and four matching nonlesional PN samples confirmed to have mutations in *NOTCH1*. Representative skin section images are shown in Figure 7A. Intensive staining for the notch intracellular domain (NICD), an indicator of active Notch signaling, was observed in both lesional and nonlesional skin of PN patients. However, NICD showed significantly higher expression in lesional dermis compared to nonlesional dermis from the same PN patients (t(3) = 5.92, $P = 0.010$, *paired Student's t-test*). There was no significant difference in NICD expression between lesional and nonlesional PN epidermis (t(3) = -0.226, $P = 0.836$) (Figure 7B and C). PN lesional skin had significantly higher co-localization of Notch1 with vimentin, a relatively specific marker for fibroblasts, compared to nonlesional skin of the same patients (t(3) = 4.77, $P = 0.018$) (Fig 7 D & E). While *NOTCH1* also co-localized with KRT10, a keratinocyte marker, there was no significant difference in co-localization between lesional and nonlesional PN skin (t(3) = -2.09), $P = 0.128$) (Figure S2).

Multi-center analysis. To test and demonstrate the clinical relevance of our findings for PN patients, we first identified the top 10 non-congenital, nonredundant diseases with the highest evidence for *NOTCH1* involvement, as determined by the gene-disease association

(GDA) score from DisGeNET (58). Highest GDAs included aortic valve calcification (0.65), precursor T-cell lymphoblastic leukemia/lymphoma (0.6), and head and neck SCC (0.6). We then leveraged a mult-center cohort through the TriNetX Research Network. 42,397 PN patients without a history of any neoplasms were identified. Controls were identified through 1:1 propensity-score matching based on age, sex, race, ethnicity, smoking status, and history of hypertension (Figure 8A; Table S3). Compared to matched controls, PN patients had a higher relative risk (RR, [95% confidence interval]) of precursor T-cell lymphoblastic leukemia/lymphoma (5.33, [2.88 to 9.88]), head and neck SCC (4.19, [3.22, 5.45]), cervical cancer (3.00, [1.85 to 4.80]), breast cancer (2.91, [2.50, 3.40]), bladder cancer (2.83, [1.924, 4.158]), connective tissue disease (2.48, [2.15, 2.87]), aortic valve calcification (1.96, [1.78, 2.18]), and aortic aneurysm (1.93, [1.680, 2.219]) (Figure 8B). There was no significant increased risk for adenoid cystic carcinoma or glioblastoma in PN patients.

Discussion

This is the first study to our knowledge to comprehensively investigate somatic mutational events in PN, and we identified recurrent nonsynonymous somatic mutations in PN lesional skin related to the Notch pathway. Increased Notch signaling was observed in PN lesional dermis, along with increased *NOTCH1* expression in fibroblasts from PN lesional skin. PN patients were also found to be at an increased risk of several *NOTCH1*-associated conditions compared to matched controls. Additional findings related to PN biology include downregulated and somatically deleted genes in PN lesional skin associated with neuronal pathways, driven by a 7q21 deletion only seen in African American PN patients. Finally, PN patients had significantly more UV-associated mutational signatures compared to AD patients, after controlling for age and race.

Our findings highlight a role for Notch signaling in PN pathology. The Notch intracellular pathway is highly conserved and plays key roles in specifying cell fates during normal tissue

development and homeostasis (59). Abnormal Notch signaling has been implicated in various human diseases and neoplasms (60). Our study identifies *NOTCH1* as the gene with most frequent nonsynonymous somatic mutations in PN. Enrichment analysis revealed that recurrently mutated genes in PN were significantly related to the Notch-mediated HES/HEY network, even after filtering genes mutated in AD controls. *NOTCH1* mutations have been strongly associated with multiple malignancies, including cSCC—a recent metanalysis of 83 cSCCs using multiple cancer gene discovery methods found *NOTCH1* as the top driver gene of cSCC (47). In the present study, *NOTCH1* was the most recurrently mutated gene in PN, and *NOTCH1* mutations significantly co-occurred with *NCOA1* mutations of the same oncogenic pathway, suggesting a proliferative attribute to PN lesional skin. Our comparison between PN and cSCC somatic data also identified *FAT1* as a recurrently mutated gene in our PN samples, another high-confidence driver of cSCC. PN patients are more likely than the general population to have coexisting health conditions, including malignancies (1, 61). In particular, we previously found PN patients at increased risk of developing SCC (25). The present study also found an association between PN and several malignancies using a multi-center cohort, and further found new associations between PN and *NOTCH1*-associated conditions.

In addition to its role in cellular proliferation, Notch signaling also has established roles in tissue fibrosis in several diseases, including renal, hepatic, pulmonary, and myocardial fibrosis (62–65). The profibrotic effect of Notch1 is likely a function of fibroblast proliferation, myofibroblast differentiation, and immune dysregulation through TGF-β signaling (30, 66, 67). Activation of Notch signaling was observed in the lesional skin of patients with systemic sclerosis, and stimulation of healthy dermal fibroblasts with a Notch1 ligand resulted in a phenotype similar to that of systemic sclerosis with increased release of collagen and differentiation of resting fibroblasts into myofibroblasts (68). Interestingly, these findings are

aligned with single-cell RNA sequencing studies indicating increased myofibroblasts in PN lesional skin (14).

Given its immunomodulating properties, hyperactive Notch signaling further contributes to fibrosis by inducing an M2 to M1 (proinflammatory) macrophage polarization, leading to myofibroblasts proliferation and recruitment of fibrocytes (69). The transition between M2 and M1 macrophages is also induced by IL-31 (70), which helps connect Notch dysregulation, inflammatory cytokine release, and itch propagation to tissue fibrosis (71, 72). Further, transcriptomic analysis of liver cancer hepatocytes shows a correlation in *NOTCH1* expression and *POSTN*, which encodes periostin (73). Periostin, an extracellular matrix protein released by skin fibroblasts, is found in the dermis of patients with PN at levels that correlate with itch intensity (74). Recent single-cell studies in PN showed significantly increased periostin in lesional skin and supports a fibroblast-neuronal axis in PN regulated by periostin (14). Hyperactivation of a compromised Notch1 receptor may be one possible mechanism by which somatic mutations in *NOTCH1* lead to the clinical cutaneous fibrosis observed in PN lesional skin. IF analysis demonstrated both significantly increased Notch signaling in lesional PN dermis and increased expression of *NOTCH1* in lesional PN skin fibroblasts. Due to its profibrotic and proinflammatory roles, and its relatively high mutation rate and activation in PN lesional skin, our study identifies *NOTCH1* as a driver in PN biology and Notch signaling as a putative target for therapeutics (60).

This study also finds significant somatic mutations in neuronal pathways. Notch1 is known to inhibit neurite outgrowth in neurons, and inhibition of hyperactive Notch signaling can reverse neurogenesis and neurite outgrowth defects (75, 76). We also observed recurrent nonsynonymous mutations in genes related to neuron projection including *MAP1B*, *TENM1*, and *CNTN2*, which were not mutated in AD. Those genes were also found to be significantly downregulated in PN lesional skin compared to nonlesional skin (10), suggesting the mutations

lead to altered neuronal structure in PN lesional skin. Further, analysis of somatic CNV in PN reveals that recurrently deleted segments affect genes which are most significantly related to neural crest development and negative regulation of axon extension.

Previous functional studies on lesional and nonlesional PN skin biopsies show altered intraepidermal and dermal nerve fiber density (77). Our mutational profiles suggest primary neuronal gene dysregulation in PN lesional skin. This is supported by association studies showing a correlation between a PN diagnosis and other systemic neuropathies (78).

Following our somatic CNV analysis, enrichment in axonal growth and guidance was largely due to a recurrent 7q21 deletion that overlaps with *SEMA3A* and related genes of the Semaphorin−plexin signaling pathway. This deletion was only observed in African American patients. This is notable in light of the disproportionate burden of PN in skin of color patients, with African Americans having a 3.4 to 4.4 times increased odds of developing PN compared to Whites (26, 61). In addition to CNV differences, we also observed unique high-VAF mutations affecting epithelial-to-mesenchymal transition African American PN patients, suggesting a distinct somatic evolutionary landscape in those patients. This is remarkable given that African Americans with PN often present much differently than Caucasian patients with more fibrotic lesions (Figure 1B and C). Previous transcriptomic studies suggest unique patterns of immune polarization in African American patients with PN (15). Somatic CNV analysis in this study adds further molecular foundation for the high rate of PN in African Americans and suggests a novel disease endotype may exist in these patients.

We observed other mutations that suggest a branch of common etiology between PN and AD. The only recurrent nonsense mutation in PN and AD was in *DUOX2*, which is involved in the release of hydrogen peroxide through NADPH oxidase (55). *DUOX2* is highly sensitive to mutation, and altered protein products have been associated with elevated plasma IL17C levels, which is characteristic of the inflammatory profiles of AD and psoriasis (55). Transcriptional and

functional studies show elevated Th17 signatures in PN patients as well, both in the skin and systemically (10, 79). However, the difference in PN is that its immunophenotype is more likely an imbalance between Th17 and Th22, with elevated levels of IL-22 (10). Interestingly, Notch signaling is shown to promote IL-22 secretion and the skewing of naïve $CD4^{+}$T cells toward Th22 cells (80). Further, Notch1 inhibition was shown to effectively alleviate the severity of psoriasis-like skin inflammation by regulating Th17 differentiation and function (81). Hyperactive Notch1 signaling can also destabilize regulatory T cells (82, 83), leaving way for unrestrained Th2-driven inflammation and itch (84). The Notch pathway was found highly mutated and hyperactive in PN lesional in this study, providing support and a genomic context to the Th17/Th22-skewed immunologic signature of PN. This is an area where precision therapeutics will make an impact, as each PN patient's treatment can be informed by their immunologic or genomic signature.

To investigate the etiology of somatic mutational processes we observed, we performed mutational signature analysis in PN and compared it to that of AD. The relative frequency of DBS1, a highly specific signature for UV exposure with frequent tandem CC>TT mutations, was significantly associated with PN. This was after controlling for age, race, and itch intensity. DBS1 significantly correlated with itch intensity in both conditions. *NOTCH1* is one of the most highly mutated genes in sun-exposed versus non-sun-exposed normal human skin samples (85), and chronic UV-A exposure was shown to expand dermal fibroblasts harboring *NOTCH1* amplifications (86). Subacute skin-barrier damage maybe an early-event in PN patients that increases susceptibility to UV-induced DNA damage, paving the way for accumulated somatic mutations and exacerbating dysregulation in the skin microenvironment. Interestingly, we did not find DBS1 associated with age. Previous work shows a similar pattern in skin fibroblasts where UV-associated DNA damage did not correlate with age, suggesting a proliferative origin (87).

We recognize some limitations in our study. First, we only sequenced samples from 17 PN cases and 10 AD controls, although PN is a relatively rare condition (61). Thus, we may have missed somatic events relevant to PN in a subset of patients. In addition, CNV analysis using WES data is limited in scope and cannot delineate all complex somatic structural variations. Nonetheless, our study represents the first and largest genomic sequencing effort for a rare and understudied disease. Our characterization of the somatic landscape in PN reveals novel insights into its pathology. Aberrant Notch signaling is identified as a likely driver in PN development, likely through profibrotic and immune deregulatory functions, with potential systemic involvement. We also provide support for the neuronal dysregulation pathophysiology of PN through identifying recurrent loss-of-function mutations in *MAP1B*, *TENM1*, and *CNTN2*, as well as recurrent copy number deletions supported by gene expression data. Finally, our mutational signature analysis revealed a strong association between DBS1 and PN, suggesting a potential role for UV-exposure in PN development or maintenance. Our findings represent much needed progress to profile PN on the molecular level.

Methods

Sample collection. Patients diagnosed with moderate-to-severe PN, with more than 20 nodules and a Worst-Itch Numeric Rating Scale (WINRS) score (88) of more than 7 out of 10 were recruited from the Johns Hopkins Itch Center. For AD controls, patients diagnosed with moderate-to-severe AD with a validated Investigator Global Assessment (vIGA) score (89) of greater than or equal to 3 and a WINRS score of more than 7 out of 10 were recruited from the Johns Hopkins Itch Center. 6-mm punch biopsies from lesional PN or AD skin and healthy, nonlesional skin within 10 cm of the nodule were collected. Half of each biopsy was formalin-fixed, paraffin-embedded (FFPE) and the other half was stored in RNALater solution (Ambion). All patients signed a consent form approved by the local Institutional Review Board.

Whole-exome analysis. Library preparation was performed with the SureSelectXT reagent kit before hybridization. SureSelect XT Human All Exon V5 library was used for hybridization. NovaSeq6000 S4 was used for sequencing 150 bp paired-end reads. Illumina's CASAVA (v1.8.4) was used to convert BCL files to FASTQ files. Initial quality control was performed using FastQC (v0.11.8). Trimgalore (v0.6.7) (90) was used to trim adapters, low-quality base calls, and short reads using default parameters. Following the “Best Practices” workflow suggested by the Broad Institute, BWA-mem (v0.7.17) (91) was used for alignment against the hg38 reference genome, Piccard-tools (v2.9.0) were used to mark duplicate reads, GATK (v3.8.0) IndelRealigner (92) was used to clean indel artifacts, and GATK BaseRecalibrator was used to recalibrate base quality scores and improve downstream variant calling. Samtools (v1.10) (93) and GATK were used to determine coverage at different levels of partitioning and aggregation. One AD sample was excluded due to low coverage (see Results). GATK MuTect2 was used to call somatic. To focus on somatic events relevant to the development of a prurigo nodule, and to further reduce the likelihood of germline calls, MuTect2 paired mode was used with lesional and nonlesional samples as the “tumor” and normal samples, respectively. The default parameters were used. Common germline variants and artifacts were filtered using a panel of normal exomes from the ExAC database; variants present in 2 or more samples within the panel of normals were removed. Somatic variants were then filtered using the following criteria: minimum phred quality of 20, minimum read depth of 20, and minimum variant allele frequency of 0.01. The functional effects of passed somatic SNVs and indels were then predicted using SnpEff (v5.0) (94). The R package Maftools (v2.21.05) (95) was used to summarize and visualize variant calls.

After variant calling, we considered excluding a hypermutated AD sample with 34,228 detected somatic variants after filtration. The rest of the AD samples had a median of 83.5 variants (range of 48 to 578). While this high number of variants might represent significant

underlying germline variation or technical artifacts, it may also reflect true hypermutation related to AD. Since this study did not focus on investigating AD pathology, and the AD variants were rather primarily used to curate a gene list that is more likely to be specific to PN somatic mutagenesis, the hypermutated AD sample was not excluded.

Gene set enrichment analysis. Enrichr (96) was used to perform gene set enrichment analysis using the following term databases: GO Biological Process, GO Cellular Component, and NCI Nature Pathways. Significant GO terms and pathways were calculated using an alpha level of 0.05 after applying the Benjamini–Hochberg correction and output was visualized in R.

Copy number analysis. Somatic CNV was inferred using CNVkit (v0.9.4) (97), using baited genomic regions for the whole-exome target capture kit S04380110 (i.e. SureSelect Human All Exon V5). Nonlesional samples were combined into a pooled reference for CNV calling, as opposed to an individual-matched analysis, which is the recommendation of the CNVkit authors for reduced CNV noise. Significantly recurrent CNV segments were identified using CNVRanger (98), which implements the statistical approach described by Beroukhim et al. to highlight regions that are aberrant more often than would be expected by chance, with greater weight assigned to high-amplitude events (homozygous deletions or high-level copy-number gains) (99).

RNA-seq data. In order to corroborate and contextualize the functional impact of somatic CNV calls, we utilized in-house gene expression data from lesional and non-lesional PN samples. Differential expression pipeline is described previously (100). Briefly, normalization and differential expression of RNA-seq data was carried out using the DESeq2 (101) R package, with adjustment for multiple hypothesis testing using Benjamini-Hochberg. Genes with adjusted-*P* less than 0.05 and $\log_2$ fold-change change < 0 or > 0 were considered down- and upregulated, respectively. A relatively permissive absolute fold-change cutoff was used to allow enrichment to be driven by somatic CNVs.

Mutational signature analysis. Mutational signatures for the landscape of single nucleotide substitution (SBS), double nucleotide substitution (DBS), and CNV across exomes were extracted based on the non-negative matrix factorization method previously described and implemented in the Sigminer R package (v2.1.7) (102, 103). CNV signatures were classified as recently described by Steele et al.; in brief, to capture biologically relevant copy number features, a CNV signature encodes the copy number profile of a sample by summing the counts of segments into a 48-dimensional vector based on total copy number, heterozygosity status, and segment size (54). The optimal number of mutational signatures to extract was determined by inspecting the cophenetic correlation coefficient, an indicator of the robustness of consensus matrix clustering, and choosing the minimal number of signatures after which the coefficient starts sharply decreasing (104). Signatures were then compared with the curated set of COSMIC signatures v3.3 (57) using cosine similarity. Signatures with less than 0.7 similarity to any known signatures in COSMIC were considered de-novo.

Mutational burden. We calculated mutational burden as the number of nonsynonymous mutations occurring per megabase of coding regions.

Shannon Diversity Index for somatic mutations. Variant-allele frequency (VAF; *v*) was inferred as the number of reads supporting the variant allele, SNV or indel, divided by the total reads supporting the reference allele and the reads supporting the variant allele. Assuming we sequenced n sites, the Shannon Diversity Index, H, for a sample was then calculated as:

$$H = -\sum_{i=1}^{n} v_i \ln v_i$$

Immunofluorescence analysis. We selected four PN patients whom we found to have *NOTCH1* mutations. Lesional and nonlesional FFPE skin samples of 5-µm thickness were deparaffinized and subjected to heat-induced antigen retrieval using Trilogy buffer (Trilogy® 920P x1, Sigma-Aldrich) and treated with DAKO protein blocking reagent (X0909, DAKO, Capinteria, CA, USA). The slides were then incubated with primary antibodies for Notch1 (ab52627, Abcam, 1:150)

and human NICD (AF3647, R&D Systems; dilution, 1:20) at 4ºC overnight, followed by reaction with conjugated secondary antibodies, DAPI intranuclear stain (62248, Thermofisher Scientific) and mounted with ProLong Glass Antifade Mountant (P36980, Thermofisher Scientific). For quantification, photomicrographs were obtained with Leica SP8 confocal microscope (Leica Microsystems, Deerfield, IL, USA) at 20x objective and x63 objective oil immersion using instrument settings. Background normalized fluorescence intensity of the antibodies in the epidermis and dermis was measured in arbitrary units (AU) using Image J software (NIH, Bethesda, MD, USA).

Gene-disease associations. We used DisGeNET (v7.0) (58) to identify diseases associated with *NOTCH1*. At the time of the study, DisGeNET had 1,134,942 gene-disease associations (GDAs) between 21,671 genes and 30,170 diseases. Their methodology ranks diseases based on a GDA score which gives a higher weight to associations reported by several expert-curated databases and with a large number of supporting publications (58). We excluded congenital conditions (e.g., bicuspid aortic valve) and redundant terms (e.g., malignant neoplasm and breast neoplasm: only breast neoplasm was included). The 10 remaining diseases with the highest GDA were then selected as *a priori* primary outcomes in our PN cohort study.

Cohort study. The TriNetX Research Network is an international, federated clinical database which contains approximately 107 million patient records at the time of this study. We first identified patients with a diagnosis of PN without any previous history of neoplasms before PN diagnosis. We utilized the International Classification of Diseases 10th Revision Clinical Modification (ICD-10-CM) code L28.1, which is given mostly by dermatologists and has been validated (105). Controls were identified through 1:1 propensity-score matching based on age, sex, race, ethnicity, smoking status, and history of hypertension. Primary outcomes were determined through corresponding ICD-10-CM codes and association was determined through

cumulative relative risk estimated using the TriNetX analytics web platform. All TriNetX analyses were completed on 02/10/2023.

Statistics. Statistical tests and visualizations were performed using R (version 4.2.0). Adjustment for false-discovery rate (FDR) due to multiple hypothesis testing was conducted using the Benjamini–Hochberg method. An alpha level of 0.05 was used to denote significance.

Study approval. This study was approved by the Johns Hopkins Institutional Review Board (IRB00231694).

Acknowledgements

S.G.K. is supported by the National Institute of Arthritis and Musculoskeletal and Skin Diseases of the National Institutes of Health under Award Number K23AR077073 and a grant from the Skin of Color Society. The content is solely the responsibility of the authors and does not necessarily represent the official views of the National Institutes of Health. We thank the Sidney Kimmel Comprehensive Cancer Center Experimental and Computational Genomics Core, receiving support through NCI grant P30CA006973, for assistance with the WES next generation sequencing studies and analysis. We also thank the PN and AD patients who donated tissue samples for this study.

Author contributions

SGK, SY, AG, YRS, MMK, TP, and AR designed the study. VP, JD, HC, AK, and SVR collected the data. AR, AG, MDS, and SW analyzed the data. HC, AK, and OO performed staining. AR and SGK wrote the first version of the manuscript. All authors reviewed and edited the manuscript.

References

1. Kwatra SG. Breaking the Itch–Scratch Cycle in Prurigo Nodularis. *N Engl J Med*. 2020;382(8):757–758.

606 2. Kwatra SG. Prurigo Nodularis. *JAMA Dermatol*. 2022;158(3):336.

607 3. Steinke S, et al. Humanistic burden of chronic pruritus in patients with inflammatory dermatoses:
608 Results of the European Academy of Dermatology and Venereology Network on Assessment of Severity
609 and Burden of Pruritus (PruNet) cross-sectional trial. *J Am Acad Dermatol*. 2018;79(3):457-463.e5.

610 4. Whang KA, et al. Health-related quality of life and economic burden of prurigo nodularis. *J Am Acad*
611 *Dermatol*. 2022;86(3):573–580.

612 5. Aggarwal P, et al. Clinical characteristics and disease burden in prurigo nodularis. *Clin Exp Dermatol*.
613 2021;46(7):1277–1284.

614 6. Whang KA, et al. Racial and Gender Differences in the Presentation of Pruritus. *Medicines*.
615 2019;6(4):98.

616 7. McColl M, et al. Pruritus in Black Skin: Unique Molecular Characteristics and Clinical Features. *J Natl*
617 *Med Assoc*. 2021;113(1):30–38.

618 8. Sutaria N, et al. Racial disparities in mortality among patients with prurigo nodularis: A multi-center
619 cohort study. *J Am Acad Dermatol*. 2022;86(2):487–490.

620 9. Wongvibulsin S, et al. A Nationwide Study of Prurigo Nodularis: Disease Burden and Healthcare
621 Utilization in the United States. *J Invest Dermatol*. 2021;141(10):2530-2533.e1.

622 10. Belzberg M, et al. Prurigo Nodularis Is Characterized by Systemic and Cutaneous T Helper 22 Immune
623 Polarization. *J Invest Dermatol*. 2021;141(9):2208-2218.e14.

624 11. Sutaria N, et al. Cutaneous Transcriptomics Identifies Fibroproliferative and Neurovascular Gene
625 Dysregulation in Prurigo Nodularis Compared with Psoriasis and Atopic Dermatitis. *J Invest Dermatol*.
626 2022;142(9):2537–2540.

627 12. Parthasarathy V, et al. Circulating plasma IL-13 and periostin are dysregulated type 2 inflammatory
628 biomarkers in prurigo nodularis: A cluster analysis. *Front Med*. 2022;9.
629 https://www.frontiersin.org/articles/10.3389/fmed.2022.1011142. Accessed February 20, 2023.

630 13. Deng J, et al. Extracellular matrix and dermal nerve growth factor dysregulation in prurigo nodularis
631 compared to atopic dermatitis. *Front Med*. 2022;9:1022889.

632 14. Patel JR, et al. Single-cell RNA sequencing reveals dysregulated fibroblast subclusters in prurigo
633 nodularis [preprint]. 2023;2023.01.29.526050.

634 15. Sutaria N, et al. Cluster Analysis of Circulating Plasma Biomarkers in Prurigo Nodularis Reveals a
635 Distinct Systemic Inflammatory Signature in African Americans. *J Invest Dermatol*. 2022;142(5):1300-
636 1308.e3.

637 16. Parthasarathy V, et al. The blood proteomic signature of prurigo nodularis (PN) reveals distinct
638 inflammatory and neuropathic endotypes: a cluster analysis. *J Am Acad Dermatol*. 2023;0(0).
639 https://doi.org/10.1016/j.jaad.2023.01.042.

640 17. Vasavda C, et al. A polygenic risk score for predicting racial and genetic susceptibility to prurigo
641 nodularis. *J Invest Dermatol*. 2023.

642 18. Brown SJ. Molecular mechanisms in atopic eczema: insights gained from genetic studies. *J Pathol*.
643 2017;241(2):140–145.

644 19. Zhou X, et al. Whole Exome Sequencing in Psoriasis Patients Contributes to Studies of Acitretin
645 Treatment Difference. *Int J Mol Sci*. 2017;18(2):295.

646 20. Olafsson S, Anderson CA. Somatic mutations provide important and unique insights into the biology
647 of complex diseases. *Trends Genet*. 2021;37(10):872–881.

648 21. Martincorena I, et al. High burden and pervasive positive selection of somatic mutations in normal
649 human skin. *Science*. 2015;348(6237):880–886.

650 22. Klonowska K, et al. Ultrasensitive profiling of UV-induced mutations identifies thousands of
651 subclinical facial tumors in tuberous sclerosis complex. *J Clin Invest*. 2022;132(10).
652 https://doi.org/10.1172/JCI155858.

653 23. Olafsson S, et al. Effects of psoriasis and psoralen exposure on the somatic mutation landscape of
654 the skin [preprint]. 2022;2022.07.04.22277086.

655 24. Nanki K, et al. Somatic inflammatory gene mutations in human ulcerative colitis epithelium. *Nature*.
656 2020;577(7789):254–259.

657 25. Larson VA, et al. Association between prurigo nodularis and malignancy in middle-aged adults. *J Am*
658 *Acad Dermatol*. 2019;81(5):1198–1201.

659 26. Boozalis E, et al. Ethnic differences and comorbidities of 909 prurigo nodularis patients. *J Am Acad*
660 *Dermatol*. 2018;79(4):714-719.e3.

661 27. Koboldt DC. Best practices for variant calling in clinical sequencing. *Genome Med*. 2020;12(1):91.

662 28. Gu C, et al. Identification of Common Genes and Pathways in Eight Fibrosis Diseases. *Front Genet*.
663 2021;11. https://www.frontiersin.org/articles/10.3389/fgene.2020.627396. Accessed September 10,
664 2022.

665 29. Sondka Z, et al. The COSMIC Cancer Gene Census: describing genetic dysfunction across all human
666 cancers. *Nat Rev Cancer*. 2018;18(11):696–705.

667 30. Condorelli AG, et al. Notch-ing up knowledge on molecular mechanisms of skin fibrosis: focus on the
668 multifaceted Notch signalling pathway. *J Biomed Sci*. 2021;28(1):36.

669 31. Fukusumi T, Califano JA. The NOTCH Pathway in Head and Neck Squamous Cell Carcinoma. *J Dent*
670 *Res*. 2018;97(6):645–653.

671 32. Sakamoto K, et al. Distinct roles of EGF repeats for the Notch signaling system. *Exp Cell Res*.
672 2005;302(2):281–291.

673 33. Remme CA. Cardiac sodium channelopathy associated with SCN5A mutations: electrophysiological,
674 molecular and genetic aspects. *J Physiol*. 2013;591(Pt 17):4099–4116.

675 34. Zhang Y, et al. Nav1.8 in keratinocytes contributes to ROS-mediated inflammation in inflammatory
676 skin diseases. *Redox Biol*. 2022;55:102427.

677 35. Shiratori-Hayashi M, et al. Astrocytic STAT3 activation and chronic itch require IP3R1/TRPC-
678 dependent Ca2+ signals in mice. *J Allergy Clin Immunol*. 2021;147(4):1341–1353.

679 36. Ma X-X, et al. PiT2 regulates neuronal outgrowth through interaction with microtubule-associated
680 protein 1B. *Sci Rep*. 2017;7(1):17850.

681 37. Verdonschot JAJ, et al. Titin cardiomyopathy leads to altered mitochondrial energetics, increased
682 fibrosis and long-term life-threatening arrhythmias. *Eur Heart J*. 2018;39(10):864–873.

683 38. Akinrinade O, Koskenvuo JW, Alastalo T-P. Prevalence of Titin Truncating Variants in General
684 Population. *PLoS ONE*. 2015;10(12):e0145284.

685 39. Wesley T, et al. The attributes of plakins in cancer and disease: perspectives on ovarian cancer
686 progression, chemoresistance and recurrence. *Cell Commun Signal*. 2021;19(1):55.

687 40. Szabo S, Wögenstein KL, Fuchs P. Functional and Genetic Analysis of Epiplakin in Epithelial Cells.
688 *Methods Enzymol*. 2016;569:261–285.

689 41. Peppino G, et al. Teneurins: Role in Cancer and Potential Role as Diagnostic Biomarkers and Targets
690 for Therapy. *Int J Mol Sci*. 2021;22(5):2321.

691 42. Stogmann E, et al. Autosomal recessive cortical myoclonic tremor and epilepsy: association with a
692 mutation in the potassium channel associated gene CNTN2. *Brain J Neurol*. 2013;136(Pt 4):1155–1160.

693 43. White AN, et al. Genetic deletion of Rgs12 in mice affects serotonin transporter expression and
694 function in vivo and ex vivo. *J Psychopharmacol Oxf Engl*. 2020;34(12):1393–1407.

695 44. Klimke W, et al. The National Center for Biotechnology Information's Protein Clusters Database.
696 *Nucleic Acids Res*. 2009;37(suppl_1):D216–D223.

697 45. Cogné B, et al. Missense Variants in the Histone Acetyltransferase Complex Component Gene TRRAP
698 Cause Autism and Syndromic Intellectual Disability. *Am J Hum Genet*. 2019;104(3):530–541.

699 46. Wei X, et al. Exome sequencing identifies GRIN2A as frequently mutated in melanoma. *Nat Genet*.
700 2011;43(5):442–446.

701 47. Chang D, Shain AH. The landscape of driver mutations in cutaneous squamous cell carcinoma. *NPJ*
702 *Genomic Med*. 2021;6(1):61.

703 48. Sanchez-Vega F, et al. Oncogenic Signaling Pathways in The Cancer Genome Atlas. *Cell*.
704 2018;173(2):321-337.e10.

705 49. Reimand J, et al. Pathway enrichment analysis and visualization of omics data using g:Profiler, GSEA,
706 Cytoscape and EnrichmentMap. *Nat Protoc*. 2019;14(2):482–517.

707 50. Hedberg ML, et al. Molecular Mechanisms of Cutaneous Squamous Cell Carcinoma. *Int J Mol Sci*.
708 2022;23(7):3478.

709 51. Su AI, et al. A gene atlas of the mouse and human protein-encoding transcriptomes. *Proc Natl Acad*
710 *Sci U S A*. 2004;101(16):6062–6067.

711 52. Stranger BE, et al. Relative Impact of Nucleotide and Copy Number Variation on Gene Expression
712 Phenotypes. *Science*. 2007;315(5813):848–853.

713 53. Zhou C, et al. Integrated Analysis of Copy Number Variations and Gene Expression Profiling in
714 Hepatocellular carcinoma. *Sci Rep*. 2017;7(1):10570.

715 54. Steele CD, et al. Signatures of copy number alterations in human cancer. *Nature*.
716 2022;606(7916):984–991.

717 55. Grasberger H, et al. DUOX2 variants associate with preclinical disturbances in microbiota-immune
718 homeostasis and increased inflammatory bowel disease risk. *J Clin Invest*. 2021;131(9).
719 https://doi.org/10.1172/JCI141676.

720 56. Guttman-Yassky E, Krueger JG. IL-17C: A Unique Epithelial Cytokine with Potential for
721 Targeting across the Spectrum of Atopic Dermatitis and Psoriasis. *J Invest Dermatol*. 2018;138(7):1467–
722 1469.

723 57. Alexandrov LB, et al. The repertoire of mutational signatures in human cancer. *Nature*.
724 2020;578(7793):94–101.

725 58. Piñero J, et al. The DisGeNET knowledge platform for disease genomics: 2019 update. *Nucleic Acids*
726 *Res*. 2020;48(D1):D845–D855.

727 59. Shen W, Huang J, Wang Y. Biological Significance of NOTCH Signaling Strength. *Front Cell Dev Biol*.
728 2021;9. https://www.frontiersin.org/articles/10.3389/fcell.2021.652273. Accessed September 25, 2022.

729 60. Allen F, Maillard I. Therapeutic Targeting of Notch Signaling: From Cancer to Inflammatory Disorders.
730 *Front Cell Dev Biol*. 2021;9. https://www.frontiersin.org/articles/10.3389/fcell.2021.649205. Accessed
731 September 8, 2022.

732 61. Huang AH, Williams KA, Kwatra SG. Prurigo nodularis: Epidemiology and clinical features. *J Am Acad*
733 *Dermatol*. 2020;83(6):1559–1565.

734 62. Yang YM, et al. Hyaluronan synthase 2-mediated hyaluronan production mediates Notch1 activation
735 and liver fibrosis. *Sci Transl Med*. 2019;11(496):eaat9284.

736 63. Yu C, et al. Histone demethylase JMJD3 protects against renal fibrosis by suppressing TGFβ and
737 Notch signaling and preserving PTEN expression. *Theranostics*. 2021;11(6):2706–2721.

738 64. Zhou Y, et al. Astragalus injection attenuates bleomycin-induced pulmonary fibrosis via down-
739 regulating Jagged1/Notch1 in lungs. *J Pharm Pharmacol*. 2016;68(3):389–396.

740 65. Lu L, et al. FSTL1-USP10-Notch1 Signaling Axis Protects Against Cardiac Dysfunction Through
741 Inhibition of Myocardial Fibrosis in Diabetic Mice. *Front Cell Dev Biol*. 2021;9:757068.

742 66. Ma S, et al. Survivin promotes rheumatoid arthritis fibroblast-like synoviocyte cell proliferation, and
743 the expression of angiogenesis-related proteins by activating the NOTCH pathway. *Int J Rheum Dis*.
744 2021;24(7):922–929.

745 67. Wang Y-C, et al. Notch1 promotes the pericyte-myofibroblast transition in idiopathic pulmonary
746 fibrosis through the PDGFR/ROCK1 signal pathway. *Exp Mol Med*. 2019;51(3):1–11.

747 68. Dees C, et al. Notch signalling regulates fibroblast activation and collagen release in systemic
748 sclerosis. *Ann Rheum Dis*. 2011;70(7):1304–1310.

749 69. Keewan E, Naser SA. Notch-1 Signaling Modulates Macrophage Polarization and Immune Defense
750 against Mycobacterium avium paratuberculosis Infection in Inflammatory Diseases. *Microorganisms*.
751 2020;8(7):1006.

752 70. Kan T, et al. IL-31 induces antitumor immunity in breast carcinoma. *J Immunother Cancer*.
753 2020;8(2):e001010.

754 71. Ständer S, et al. Trial of Nemolizumab in Moderate-to-Severe Prurigo Nodularis. *N Engl J Med*.
755 2020;382(8):706–716.

756 72. Deng J, et al. Modulation of Neuroimmune and Epithelial Dysregulation in Patients With Moderate to
757 Severe Prurigo Nodularis Treated With Nemolizumab. *JAMA Dermatol*. 2023;e232609.

758 73. Kongkavitoon P, et al. Regulation of periostin expression by Notch signaling in hepatocytes and liver
759 cancer cell lines. *Biochem Biophys Res Commun*. 2018;506(3):739–745.

74. Hashimoto T, et al. Dermal Periostin: A New Player in Itch of Prurigo Nodularis. *Acta Derm Venereol*. 2021;101(1):adv00375.

75. Berezovska O, et al. Notch1 inhibits neurite outgrowth in postmitotic primary neurons. *Neuroscience*. 1999;93(2):433–439.

76. Winanto, et al. Organoid cultures of MELAS neural cells reveal hyperactive Notch signaling that impacts neurodevelopment. *Cell Death Dis*. 2020;11(3):1–8.

77. Schuhknecht B, et al. Reduced intraepidermal nerve fibre density in lesional and nonlesional prurigo nodularis skin as a potential sign of subclinical cutaneous neuropathy. *Br J Dermatol*. 2011;165(1):85–91.

78. Hughes J-DM, et al. Association between Prurigo Nodularis and Etiologies of Peripheral Neuropathy: Suggesting a Role for Neural Dysregulation in Pathogenesis. *Medicines*. 2020;7(1):4.

79. Wong L-S, et al. IL-17A Induces Endothelin-1 Expression through p38 Pathway in Prurigo Nodularis. *J Invest Dermatol*. 2020;140(3):702-706.e2.

80. Zeng C, et al. The NOTCH-HES-1 axis is involved in promoting Th22 cell differentiation. *Cell Mol Biol Lett*. 2021;26(1):7.

81. Ma L, et al. Effect of γ-secretase inhibitor on Th17 cell differentiation and function of mouse psoriasis-like skin inflammation. *J Transl Med*. 2018;16(1):59.

82. Benamar M, et al. The Notch1/CD22 signaling axis disrupts Treg function in SARS-CoV-2–associated multisystem inflammatory syndrome in children. *J Clin Invest*. 2023;133(1). https://doi.org/10.1172/JCI163235.

779 83. Rivas MN, Arditi M. Notch1 signaling impairs regulatory T cells during multisystem inflammatory
780 syndrome in children. *J Clin Invest*. 2023;133(1). https://doi.org/10.1172/JCI166016.

781 84. Singer BD, D'Alessio FR. Regulatory T cell Itch reins in Th2 inflammation. *Cell Mol Immunol*.
782 2014;11(2):126–128.

783 85. Wei L, et al. Ultradeep sequencing differentiates patterns of skin clonal mutations associated with
784 sun-exposure status and skin cancer burden. *Sci Adv*. 2021;7(1):eabd7703.

785 86. Katarkar A, et al. NOTCH1 gene amplification promotes expansion of Cancer Associated Fibroblast
786 populations in human skin. *Nat Commun*. 2020;11(1):5126.

787 87. Abyzov A, et al. One thousand somatic SNVs per skin fibroblast cell set baseline of mosaic mutational
788 load with patterns that suggest proliferative origin. *Genome Res*. 2017;27(4):512–523.

789 88. Ständer S, et al. Worst itch numerical rating scale for prurigo nodularis: a psychometric evaluation. *J*
790 *Eur Acad Dermatol Venereol JEADV*. 2022;36(4):573–581.

791 89. Simpson E, et al. The Validated Investigator Global Assessment for Atopic Dermatitis (vIGA-AD): The
792 development and reliability testing of a novel clinical outcome measurement instrument for the severity
793 of atopic dermatitis. *J Am Acad Dermatol*. 2020;83(3):839–846.

794 90. Martin M. Cutadapt removes adapter sequences from high-throughput sequencing reads.
795 *EMBnet.journal*. 2011;17(1):10–12.

796 91. Fast and accurate short read alignment with Burrows–Wheeler transform | Bioinformatics | Oxford
797 Academic [Internet]. https://academic.oup.com/bioinformatics/article/25/14/1754/225615. Accessed
798 September 18, 2022.

799 92. McKenna A, et al. The Genome Analysis Toolkit: A MapReduce framework for analyzing next-
800 generation DNA sequencing data. *Genome Res*. 2010;20(9):1297–1303.

801 93. Li H, et al. The Sequence Alignment/Map format and SAMtools. *Bioinformatics*. 2009;25(16):2078–
802 2079.

803 94. Cingolani P, et al. A program for annotating and predicting the effects of single nucleotide
804 polymorphisms, SnpEff: SNPs in the genome of Drosophila melanogaster strain w ^{1118}; iso-2; iso-3. *Fly*
805 *(Austin)*. 2012;6(2):80–92.

806 95. Mayakonda A, et al. Maftools: efficient and comprehensive analysis of somatic variants in cancer.
807 *Genome Res*. 2018;28(11):1747–1756.

808 96. Kuleshov MV, et al. Enrichr: a comprehensive gene set enrichment analysis web server 2016 update.
809 *Nucleic Acids Res*. 2016;44(Web Server issue):W90–W97.

810 97. Talevich E, et al. CNVkit: Genome-Wide Copy Number Detection and Visualization from Targeted
811 DNA Sequencing. *PLOS Comput Biol*. 2016;12(4):e1004873.

812 98. da Silva V, et al. CNVRanger: association analysis of CNVs with gene expression and quantitative
813 phenotypes. *Bioinformatics*. 2020;36(3):972–973.

814 99. Beroukhim R, et al. Assessing the significance of chromosomal aberrations in cancer: Methodology
815 and application to glioma. *Proc Natl Acad Sci*. 2007;104(50):20007–20012.

816 100. Belzberg M, et al. Prurigo Nodularis Is Characterized by Systemic and Cutaneous T Helper 22
817 Immune Polarization. *J Invest Dermatol*. 2021;141(9):2208-2218.e14.

818 101. Love MI, Huber W, Anders S. Moderated estimation of fold change and dispersion for RNA-seq data
819 with DESeq2. *Genome Biol*. 2014;15(12):550.

820 102. Alexandrov LB, et al. Deciphering signatures of mutational processes operative in human cancer.
821 *Cell Rep*. 2013;3(1):246–259.

822 103. Wang S, et al. Sigflow: an automated and comprehensive pipeline for cancer genome mutational
823 signature analysis. *Bioinformatics*. 2021;37(11):1590–1592.

824 104. Gaujoux R, Seoighe C. A flexible R package for nonnegative matrix factorization. *BMC*
825 *Bioinformatics*. 2010;11(1):367.

826 105. Roh YS, et al. Validation of International Classification of Diseases Tenth Revision code for prurigo
827 nodularis. *J Am Acad Dermatol*. 2022;87(2):482–484.

828

829

Figure 1. Somatic mutational landscape of PN. (A) Schematic of the study design including sample collection and analysis. (B, C) Example skin images of two patients with prurigo nodularis (PN) enrolled in this study. (B) Dorsal left arm of an African American patient with scattered prurigo nodules. (C) Right arm of a Caucasian patient with scattered prurigo nodules. (D) Demographic information of PN and atopic dermatitis (AD) patients. (E) Waterfall plot displaying somatic mutations in 15 of the most frequently mutated genes in PN lesional skin compared to nonlesional skin. Ties were broken by known gene function. Columns represent the 17 PN patients. Numbers shown on the right indicate the frequency of gene mutation. Total nonsynonymous somatic SNPs and indels per sample are displayed on top. One sample was hypermutated with 450 mutations. Bottom plot shows the frequency of different classes of SNVs. Variants annotated as Multi Hit are those genes which mutated more than once in the same sample. (F) Total number of somatic mutations per sample, broken down by predicted impact on protein product based on snpEff, with functional (High or Moderate) impact in yellow and nonfunctional (Low or Modifier) in blue. (G) Boxplot showing the variant allele frequency (VAF) of nonsynonymous somatic mutations across race. (H) **, $P < 0.01$.

Figure 2. Distinct somatic selection in lesional skin of African American patients with PN. (A) Nonsynonymous somatic mutations are ordered by their genomic locations on the x-axis and the corresponding VAF is shown on the y-axis. Variants with 0.3 or higher VAF are labelled with their gene name. (B and C) Bar graph showing the pathway enrichment results of high-VAF (>0.3) nonsynonymous mutations in African American and Caucasian PN patients, respectively.

Figure 3. Co-occurrence and enrichment of recurrent somatic mutations in PN lesional skin. (A) Somatic mutational correlation matrix of all 46 genes with recurrent nonsynonymous somatic mutations in PN lesional skin. Significant pairs were identified with Fisher's exact test. (B-D) Gene ontology (GO) term and pathway enrichment results of recurrently-mutated genes across three pathway databases. Terms with FDR-corrected $P < 0.05$ are colored in yellow.

Figure 4. Somatic mutations in PN and cSCC. (A) Rank order plot showing the somatic mutational burden (number of nonsynonymous mutations occurring per megabase of coding regions) across 17 PN patients and 83 cutaneous squamous cell carcinoma (cSCC) patients. Red dashed line indicates the median mutational burden. Inset is a boxplot comparison of somatic mutational burden between the two cohorts. (B) Boxplot showing VAF of all nonsynonymous somatic variants in cSCC and PN patients. (C) Venn diagram depicting the overlap between known cSCC driver genes, genes that were found mutated in 25% or more of the 83 cSCC samples (cSCC recurrent), and genes that were found mutated in 2 or more of our 17 PN samples (PN lesional recurrent). (D, E) Somatic mutations falling within the *NOTCH1* and *FAT1*, respectively. y-axis indicates the number of PN (top) or cSCC (bottom) patients the carrying the somatic mutation. Colored rectangles indicate known functional domains of the protein product. EGF, epidermal growth factor; LamG, laminin G.

Figure 5. Landscape of somatic CNV in PN. (A) Normalized copy number per sample per chromosome for African American and Caucasian patients. (B) Circular plot illustrating the proportion of samples with deletions (red) and duplications (blue) per genomic region for African American patients (outer ideogram)

and Caucasian patients (inner ideogram). (C) Examples of recurrent somatic CNV events only observed in African American patients or Caucasian patients on chromosomes 12 and 15, respectively. (D) RNA-seq data was used to determine differentially down- and up-regulated genes in PN lesional skin. Transcript log2 fold-change is shown on the y-axis with respect to genomic location on chromosome 7 on the x-axis. Overlayed red box shows the location of the recurrent 7q21 somatic deletion. (E) GO term enrichment results of 264 genes that overlapped recurrent deletions while also being differentially downregulated in PN lesional skin. Terms with FDR-corrected $P < 0.05$ are colored in yellow. (F) Decomposition plot showing the relative contributions of CNV signature components to the three somatic CNV signatures detected (HomDel: homozygous deletion, LOH: loss-of-heterozygosity). (G) Distribution of CNV signatures in African American and Caucasian PN patients.

Figure 6. Somatic mutational differences between PN and AD. (A) Ten genes with the most frequent nonsynonymous somatic mutations in our AD cohort. (B) All nonsynonymous somatic mutations in AD and PN are ordered by their genomic locations on the x-axis and the corresponding VAF is shown on the y-axis. Variants with 0.3 or higher VAF are labelled with their gene name. (C) Histograms showing the frequency of nonsynonymous somatic variants on the x-axis at the corresponding VAF on the y-axis, in AD and PN. *P*-value indicates the significant difference in means (*Wilcoxon*). (D) Mutational diversity per sample using a normalized Shannon Diversity Index based on the VAF of somatic SNVs and indels in PN and AD patients. One hypermutated AD sample was not excluded (see Methods). (E) The top mutated genes in our PN cohort are illustrated, with the corresponding relative frequency and percentage of alteration in AD and PN samples. (F) Rank order plot showing the somatic mutational burden per megabase across 17 PN patients, 9 AD patients, and all 33 cancers in The Cancer Genome Atlas cohort. Red lines indicate the median mutational burden. A dictionary for cancer symbols is included in Table S3 (G, H) GO term enrichment results of 21 genes with nonsynonymous somatic mutations in at least two PN samples and no AD samples across two pathway databases. Terms with FDR-corrected $P < 0.05$ are colored in yellow.

Figure 7. Somatic mutational signatures in PN and AD. (A) Decomposition plot of the 4 somatic SBS signatures detected showing the relative proportion of each transition and transversion subtype. (B) Distribution of SBS signatures in PN and AD samples. The inset figure shows the relative exposures of mutational signature types. Not shown, but included in all analyses, is a hypermutated AD sample with >20,000 instances of SBS5. (C) Boxplot showing the distribution of SBS signatures in PN compared to AD. (D) Decomposition plot of the two somatic DBS signatures detected showing the relative proportion of each base-pair mutation subtype. (E) Distribution of DBS signatures in PN and AD samples. The inset figure shows the relative exposures of DBS signature types. Samples not shown did not display any known DBS signatures (E) Partial regression plots of DBS1 on each of age, race, itch intensity, and condition (PN versus AD), after controlling for the remaining covariates. Overall model adjusted $R^2 = 0.66$.

Figure 8. Notch signaling is activated in lesional skin of PN patients. (A) IF staining of NICD in lesional and nonlesional skin sections of a PN patient with a *NOTCH1* somatic mutation. Representative skin sections are shown at 189-fold magnification of the dermis. NICD (green), DAPI (blue). (B & C) Paired boxplot showing the difference in relative expression of NICD between lesional and nonlesional PN dermis (B) and epidermis (C). (D) IF staining of Notch1 and vimentin in lesional and nonlesional skin sections of a PN patient. Notch1 (red), vimentin (green), DAPI (blue). Representative skin sections are shown at 189-fold magnification of the dermis. (E) Paired boxplot showing the difference in relative co-localization of Notch1 and vimentin between PN lesional and nonlesional skin.

Figure 9. Higher risk of *NOTCH1*-associated diseases in PN patients. (A) A multi-center cohort of PN patients and propensity-score matched controls was obtained using the TriNetX Research Network. The top 10 acquired, non-redundant diseases associated with *NOTCH1* were determined based on available literature support using the DisGeNET database (B) Cumulative relative risk of *NOTCH1*-associated diseases in PN patients compared to matched controls. LL/L, lymphoblastic leukemia/lymphoma; H&N SCC, head and neck squamous cell carcinoma; ***, $P < 0.0001$; ns, no significant difference in risk.

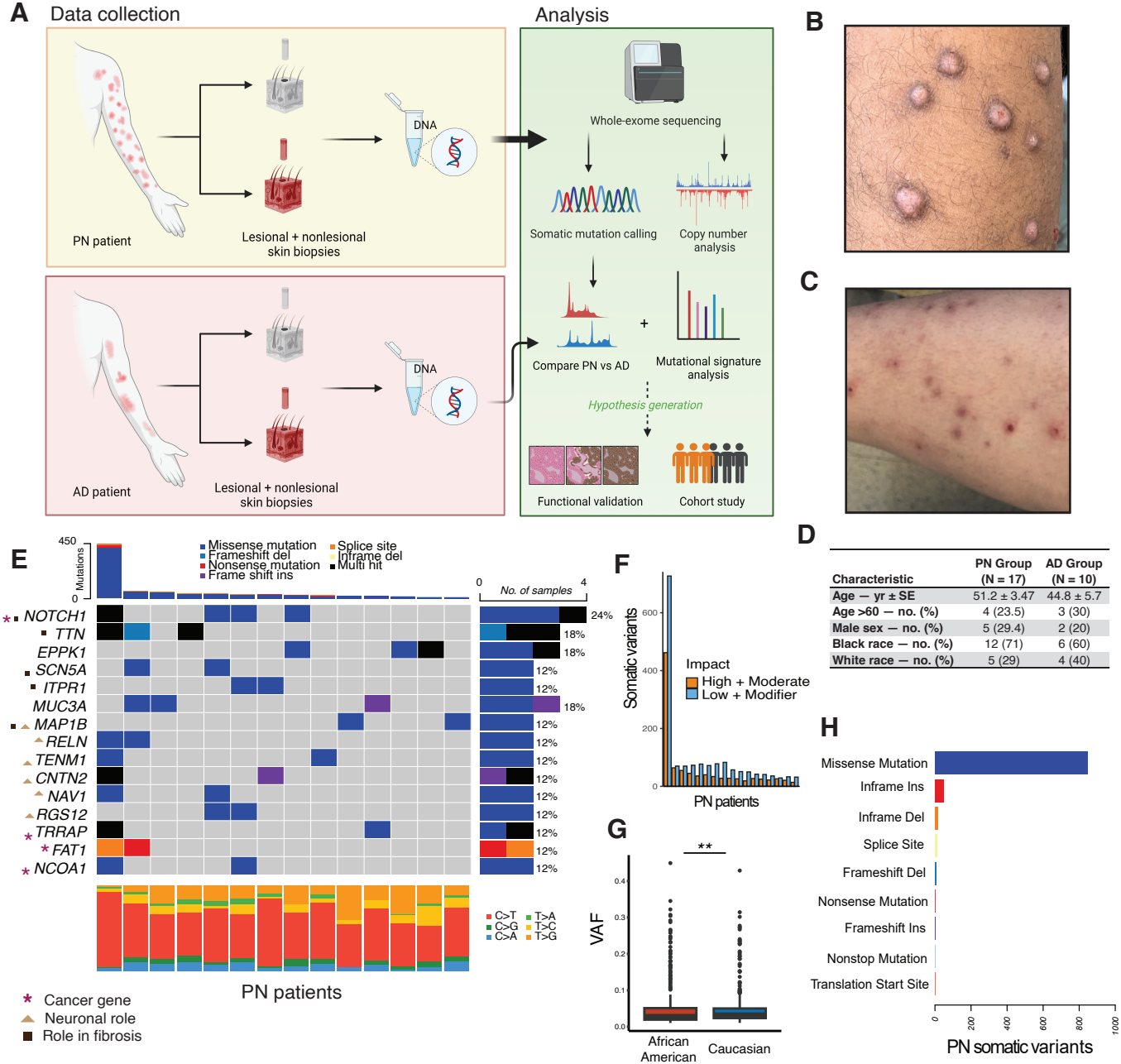
A
Data collection
Analysis
PN patient
Lesional + nonlesional skin biopsies
DNA
AD patient
Lesional + nonlesional skin biopsies
DNA
Whole-exome sequencing
Somatic mutation calling
Copy number analysis
Compare PN vs AD
Mutational signature analysis
Hypothesis generation
Functional validation
Cohort study
B
C
D
Characteristic | PN Group (N = 17) | AD Group (N = 10)
Age — yr ± SE | 51.2 ± 3.47 | 44.8 ± 5.7
Age >60 — no. (%) | 4 (23.5) | 3 (30)
Male sex — no. (%) | 5 (29.4) | 2 (20)
Black race — no. (%) | 12 (71) | 6 (60)
White race — no. (%) | 5 (29) | 4 (40)
E
Mutations
Missense mutation
Frameshift del
Nonsense mutation
Frame shift ins
Splice site
Inframe del
Multi hit
No. of samples
NOTCH1
TTN
EPPK1
SCN5A
ITPR1
MUC3A
MAP1B
RELN
TENM1
CNTN2
NAV1
RGS12
TRRAP
FAT1
NCOA1
24%
18%
18%
12%
12%
18%
12%
12%
12%
12%
12%
12%
12%
12%
12%
C>T
C>G
C>A
T>A
T>C
T>G
PN patients
Cancer gene
Neuronal role
Role in fibrosis
F
Somatic variants
Impact
High + Moderate
Low + Modifier
PN patients
G
VAF
**
African American
Caucasian
H
Missense Mutation
Inframe Ins
Inframe Del
Splice Site
Frameshift Del
Nonsense Mutation
Frameshift Ins
Nonstop Mutation
Translation Start Site
PN somatic variants

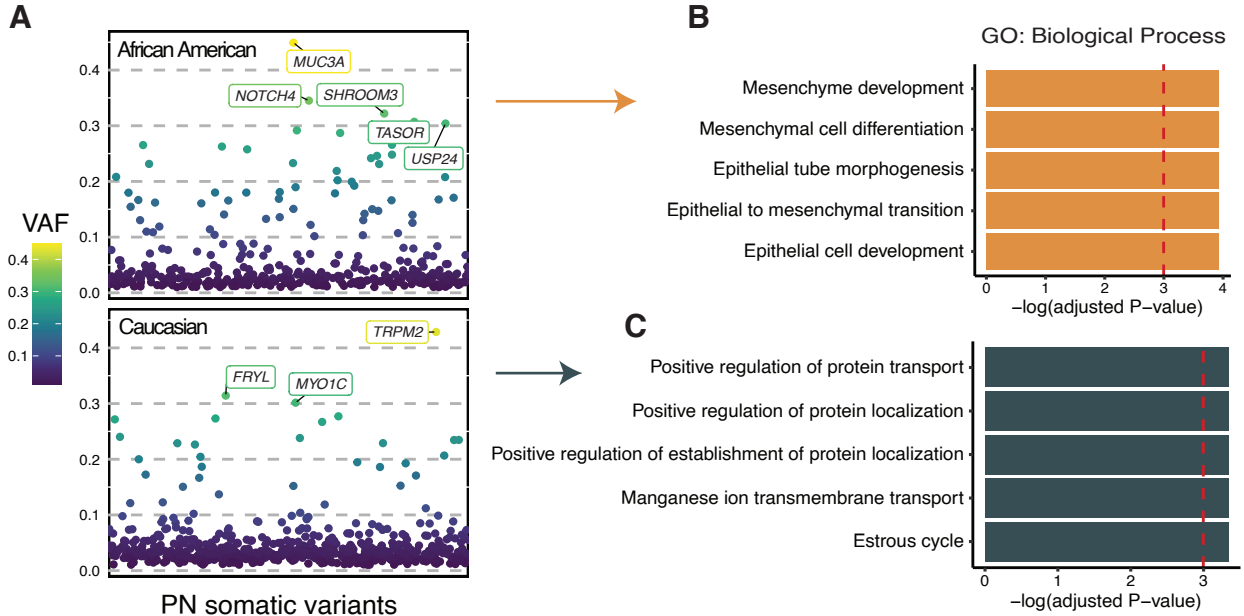
A
African American
MUC3A
NOTCH4
SHROOM3
TASOR
USP24
Caucasian
TRPM2
FRYL
MYO1C
VAF
0.4
0.3
0.2
0.1
0.0
PN somatic variants
B
GO: Biological Process
Mesenchyme development
Mesenchymal cell differentiation
Epithelial tube morphogenesis
Epithelial to mesenchymal transition
Epithelial cell development
0
1
2
3
4
−log(adjusted P−value)
C
Positive regulation of protein transport
Positive regulation of protein localization
Positive regulation of establishment of protein localization
Manganese ion transmembrane transport
Estrous cycle
0
1
2
3
−log(adjusted P−value)

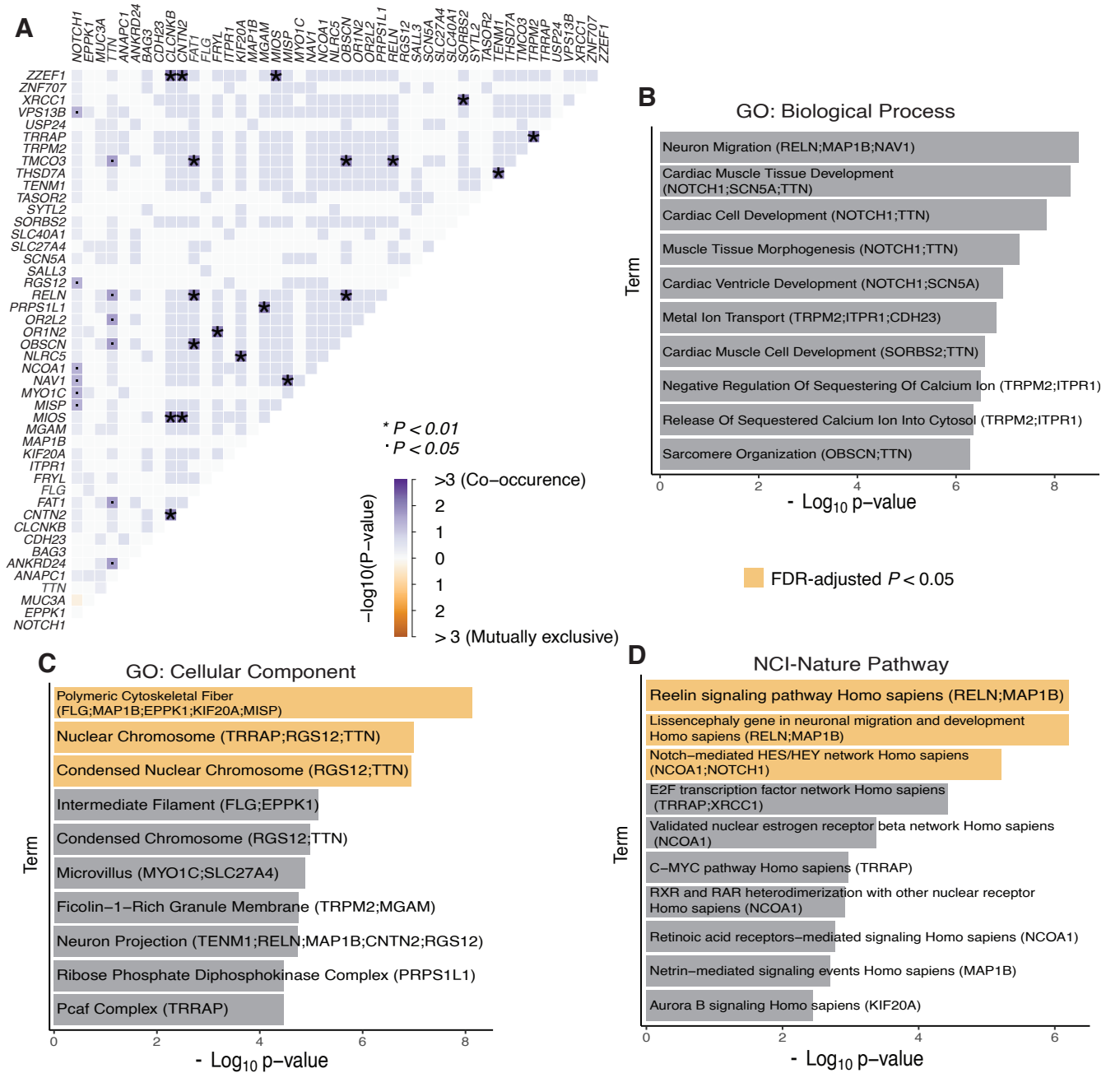
A
NOTCH1
EPPK1
MUC3A
TTN
ANAPC1
ANKRD24
BAG3
CDH23
CLCNKB
CNTN2
FAT1
FLG
FRYL
ITPR1
KIF20A
MAP1B
MGAM
MIOS
MISP
MYO1C
NAV1
NCOA1
NLRC5
OBSCN
OR1N2
OR2L2
PRPS1L1
RELN
RGS12
SALL3
SCN5A
SLC27A4
SLC40A1
SORBS2
SYTL2
TASOR2
TENM1
THSD7A
TMCO3
TRPM2
TRRAP
USP24
VPS13B
XRCC1
ZNF707
ZZEF1
* P < 0.01
· P < 0.05
−log10(P−value)
>3 (Co−occurence)
2
1
0
1
2
> 3 (Mutually exclusive)
B
GO: Biological Process
Neuron Migration (RELN;MAP1B;NAV1)
Cardiac Muscle Tissue Development (NOTCH1;SCN5A;TTN)
Cardiac Cell Development (NOTCH1;TTN)
Muscle Tissue Morphogenesis (NOTCH1;TTN)
Cardiac Ventricle Development (NOTCH1;SCN5A)
Metal Ion Transport (TRPM2;ITPR1;CDH23)
Cardiac Muscle Cell Development (SORBS2;TTN)
Negative Regulation Of Sequestering Of Calcium Ion (TRPM2;ITPR1)
Release Of Sequestered Calcium Ion Into Cytosol (TRPM2;ITPR1)
Sarcomere Organization (OBSCN;TTN)
Term
0
2
4
6
8
- Log10 p−value
FDR-adjusted P < 0.05
C
GO: Cellular Component
Polymeric Cytoskeletal Fiber (FLG;MAP1B;EPPK1;KIF20A;MISP)
Nuclear Chromosome (TRRAP;RGS12;TTN)
Condensed Nuclear Chromosome (RGS12;TTN)
Intermediate Filament (FLG;EPPK1)
Condensed Chromosome (RGS12;TTN)
Microvillus (MYO1C;SLC27A4)
Ficolin−1−Rich Granule Membrane (TRPM2;MGAM)
Neuron Projection (TENM1;RELN;MAP1B;CNTN2;RGS12)
Ribose Phosphate Diphosphokinase Complex (PRPS1L1)
Pcaf Complex (TRRAP)
Term
0
2
4
6
8
- Log10 p−value
D
NCI-Nature Pathway
Reelin signaling pathway Homo sapiens (RELN;MAP1B)
Lissencephaly gene in neuronal migration and development Homo sapiens (RELN;MAP1B)
Notch−mediated HES/HEY network Homo sapiens (NCOA1;NOTCH1)
E2F transcription factor network Homo sapiens (TRRAP;XRCC1)
Validated nuclear estrogen receptor beta network Homo sapiens (NCOA1)
C−MYC pathway Homo sapiens (TRRAP)
RXR and RAR heterodimerization with other nuclear receptor Homo sapiens (NCOA1)
Retinoic acid receptors−mediated signaling Homo sapiens (NCOA1)
Netrin−mediated signaling events Homo sapiens (MAP1B)
Aurora B signaling Homo sapiens (KIF20A)
Term
0
2
4
6
- Log10 p−value

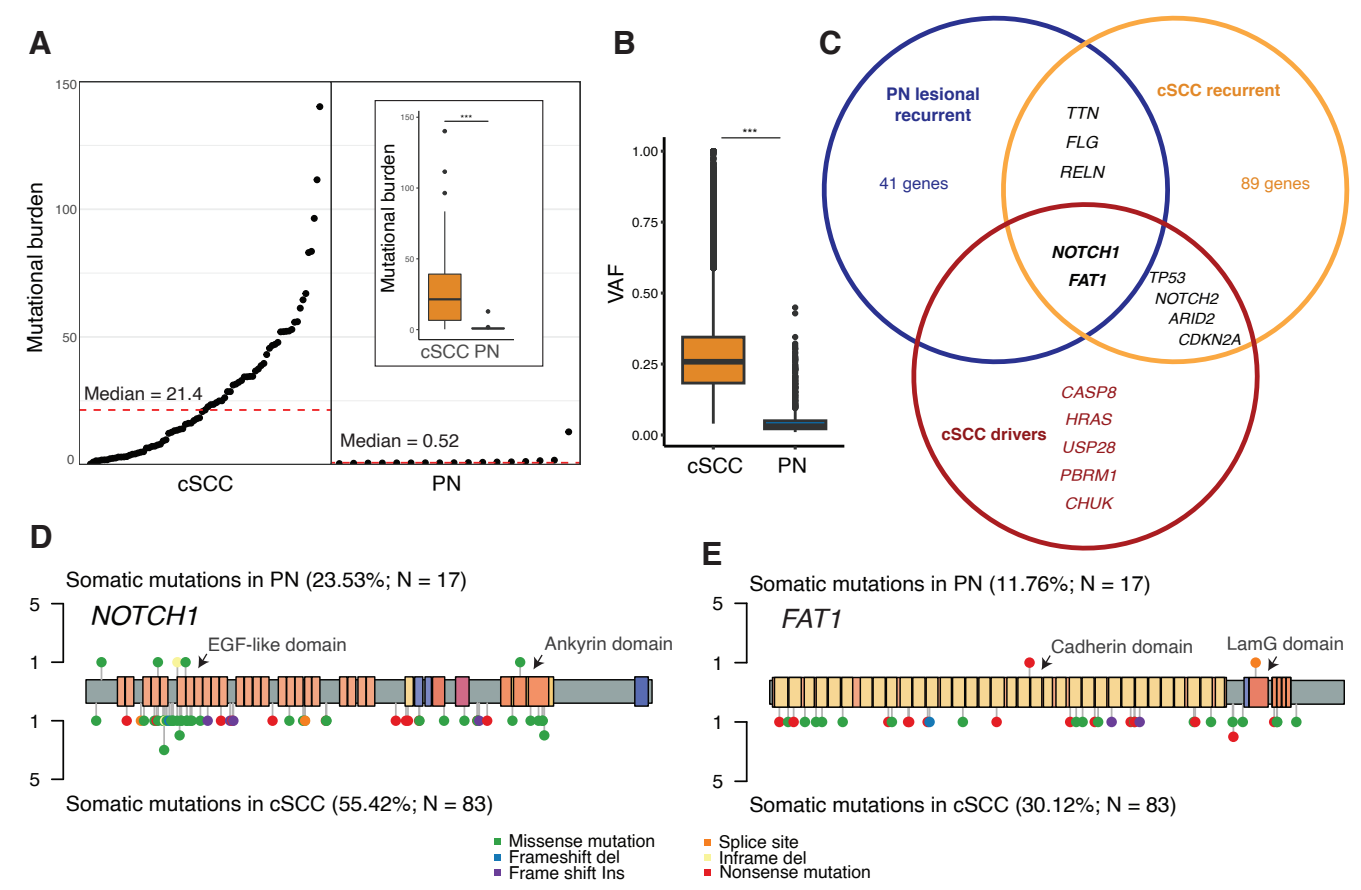
A
Mutational burden
150
100
50
0
Median = 21.4
Median = 0.52
cSCC
PN
Mutational burden
***
cSCC PN
B
VAF
1.00
0.75
0.50
0.25
0.00
***
cSCC
PN
C
PN lesional recurrent
41 genes
cSCC recurrent
89 genes
TTN
FLG
RELN
NOTCH1
FAT1
TP53
NOTCH2
ARID2
CDKN2A
cSCC drivers
CASP8
HRAS
USP28
PBRM1
CHUK
D
Somatic mutations in PN (23.53%; N = 17)
NOTCH1
EGF-like domain
Ankyrin domain
5
1
1
5
Somatic mutations in cSCC (55.42%; N = 83)
E
Somatic mutations in PN (11.76%; N = 17)
FAT1
Cadherin domain
LamG domain
5
1
1
5
Somatic mutations in cSCC (30.12%; N = 83)
Missense mutation
Frameshift del
Frame shift Ins
Splice site
Inframe del
Nonsense mutation

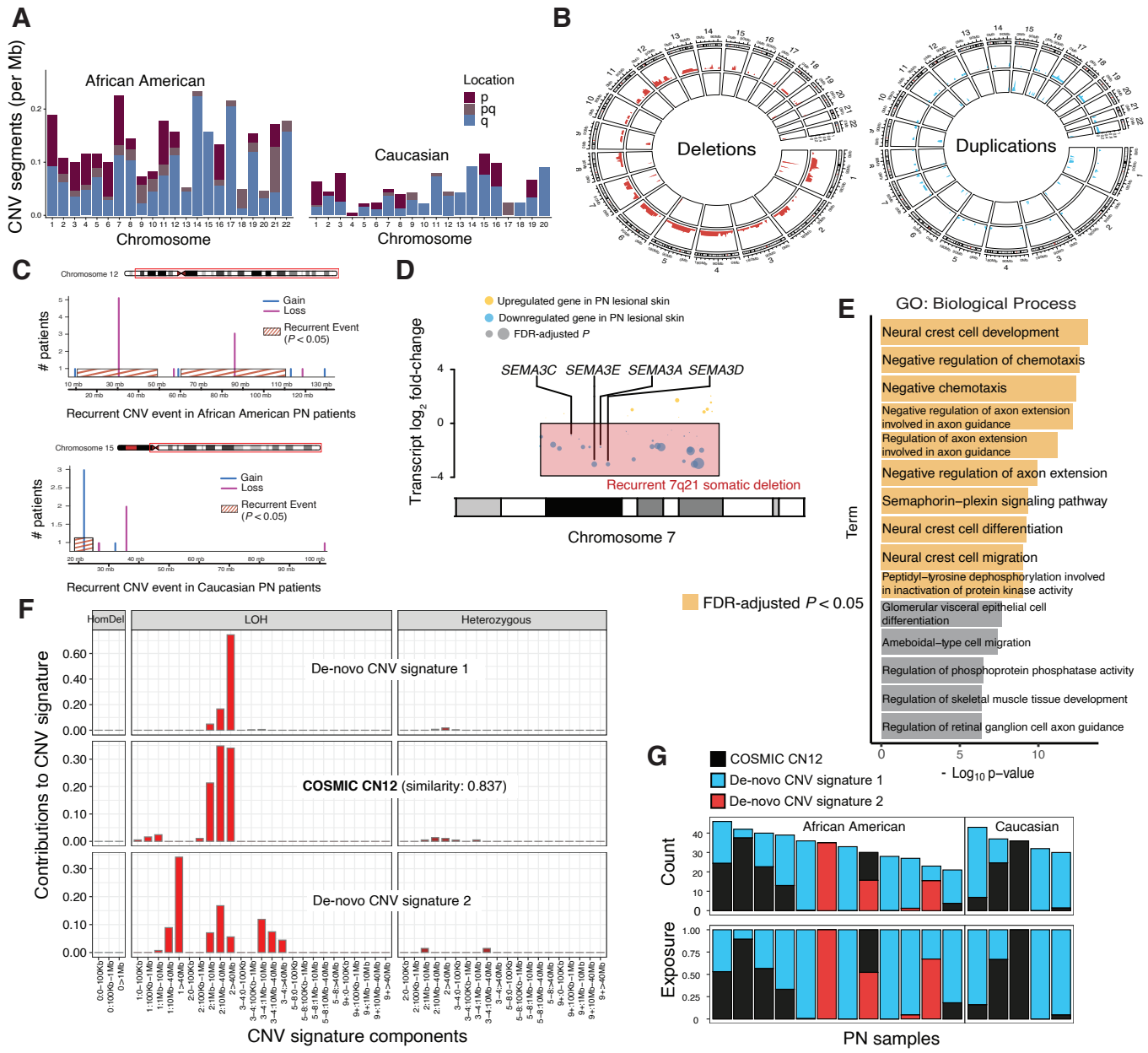
A
CNV segments (per Mb)
African American
Caucasian
Location
p
pq
q
Chromosome
Chromosome
B
Deletions
Duplications
C
Chromosome 12
patients
Gain
Loss
Recurrent Event
(P < 0.05)
Recurrent CNV event in African American PN patients
Chromosome 15
patients
Gain
Loss
Recurrent Event
(P < 0.05)
Recurrent CNV event in Caucasian PN patients
D
Upregulated gene in PN lesional skin
Downregulated gene in PN lesional skin
FDR-adjusted P
Transcript log2 fold-change
SEMA3C SEMA3E SEMA3A SEMA3D
Recurrent 7q21 somatic deletion
Chromosome 7
E
GO: Biological Process
Neural crest cell development
Negative regulation of chemotaxis
Negative chemotaxis
Negative regulation of axon extension involved in axon guidance
Regulation of axon extension involved in axon guidance
Negative regulation of axon extension
Semaphorin–plexin signaling pathway
Neural crest cell differentiation
Neural crest cell migration
Peptidyl–tyrosine dephosphorylation involved in inactivation of protein kinase activity
Glomerular visceral epithelial cell differentiation
Ameboidal–type cell migration
Regulation of phosphoprotein phosphatase activity
Regulation of skeletal muscle tissue development
Regulation of retinal ganglion cell axon guidance
Term
FDR-adjusted P < 0.05
- Log10 p–value
F
HomDel
LOH
Heterozygous
De-novo CNV signature 1
COSMIC CN12 (similarity: 0.837)
De-novo CNV signature 2
Contributions to CNV signature
CNV signature components
G
COSMIC CN12
De-novo CNV signature 1
De-novo CNV signature 2
African American
Caucasian
Count
Exposure
PN samples

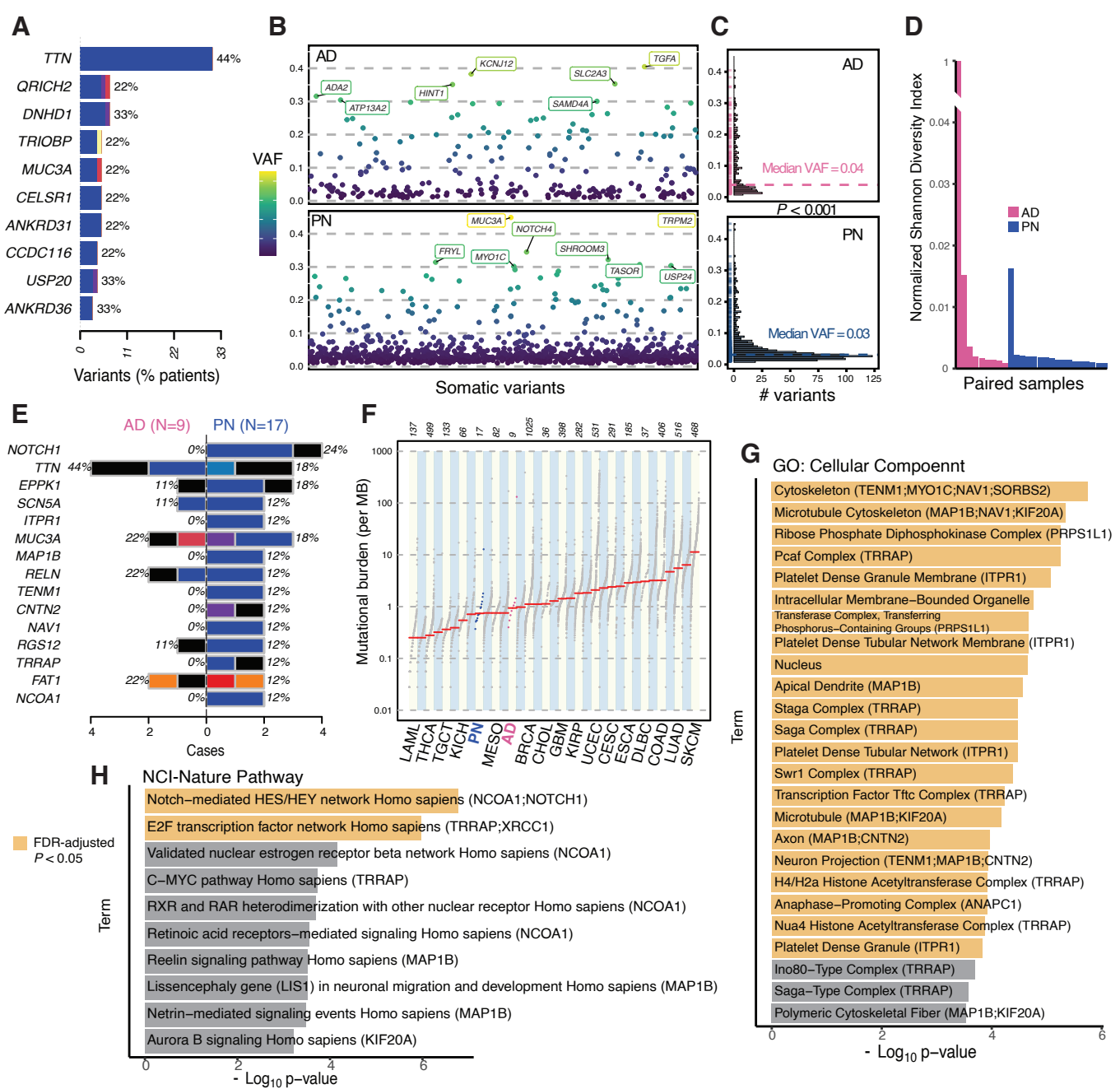
A
TTN
QRICH2
DNHD1
TRIOBP
MUC3A
CELSR1
ANKRD31
CCDC116
USP20
ANKRD36
44%
22%
33%
22%
22%
22%
22%
22%
33%
33%
0
11
22
33
Variants (% patients)
B
AD
PN
VAF
KCNJ12
TGFA
SLC2A3
ADA2
HINT1
ATP13A2
SAMD4A
MUC3A
NOTCH4
TRPM2
FRYL
MYO1C
SHROOM3
TASOR
USP24
Somatic variants
C
AD
PN
Median VAF = 0.04
P < 0.001
Median VAF = 0.03
variants
D
Normalized Shannon Diversity Index
AD
PN
Paired samples
E
AD (N=9)
PN (N=17)
NOTCH1
TTN
EPPK1
SCN5A
ITPR1
MUC3A
MAP1B
RELN
TENM1
CNTN2
NAV1
RGS12
TRRAP
FAT1
NCOA1
Cases
F
Mutational burden (per MB)
LAML
THCA
TGCT
KICH
PN
MESO
AD
BRCA
CHOL
GBM
KIRP
UCEC
CESC
ESCA
DLBC
COAD
LUAD
SKCM
G
GO: Cellular Compoennt
Cytoskeleton (TENM1;MYO1C;NAV1;SORBS2)
Microtubule Cytoskeleton (MAP1B;NAV1;KIF20A)
Ribose Phosphate Diphosphokinase Complex (PRPS1L1)
Pcaf Complex (TRRAP)
Platelet Dense Granule Membrane (ITPR1)
Intracellular Membrane−Bounded Organelle
Transferase Complex, Transferring Phosphorus−Containing Groups (PRPS1L1)
Platelet Dense Tubular Network Membrane (ITPR1)
Nucleus
Apical Dendrite (MAP1B)
Staga Complex (TRRAP)
Saga Complex (TRRAP)
Platelet Dense Tubular Network (ITPR1)
Swr1 Complex (TRRAP)
Transcription Factor Tftc Complex (TRRAP)
Microtubule (MAP1B;KIF20A)
Axon (MAP1B;CNTN2)
Neuron Projection (TENM1;MAP1B;CNTN2)
H4/H2a Histone Acetyltransferase Complex (TRRAP)
Anaphase−Promoting Complex (ANAPC1)
Nua4 Histone Acetyltransferase Complex (TRRAP)
Platelet Dense Granule (ITPR1)
Ino80−Type Complex (TRRAP)
Saga−Type Complex (TRRAP)
Polymeric Cytoskeletal Fiber (MAP1B;KIF20A)
Term
- Log10 p−value
H
NCI-Nature Pathway
FDR-adjusted P < 0.05
Notch−mediated HES/HEY network Homo sapiens (NCOA1;NOTCH1)
E2F transcription factor network Homo sapiens (TRRAP;XRCC1)
Validated nuclear estrogen receptor beta network Homo sapiens (NCOA1)
C−MYC pathway Homo sapiens (TRRAP)
RXR and RAR heterodimerization with other nuclear receptor Homo sapiens (NCOA1)
Retinoic acid receptors−mediated signaling Homo sapiens (NCOA1)
Reelin signaling pathway Homo sapiens (MAP1B)
Lissencephaly gene (LIS1) in neuronal migration and development Homo sapiens (MAP1B)
Netrin−mediated signaling events Homo sapiens (MAP1B)
Aurora B signaling Homo sapiens (KIF20A)
Term
- Log10 p−value

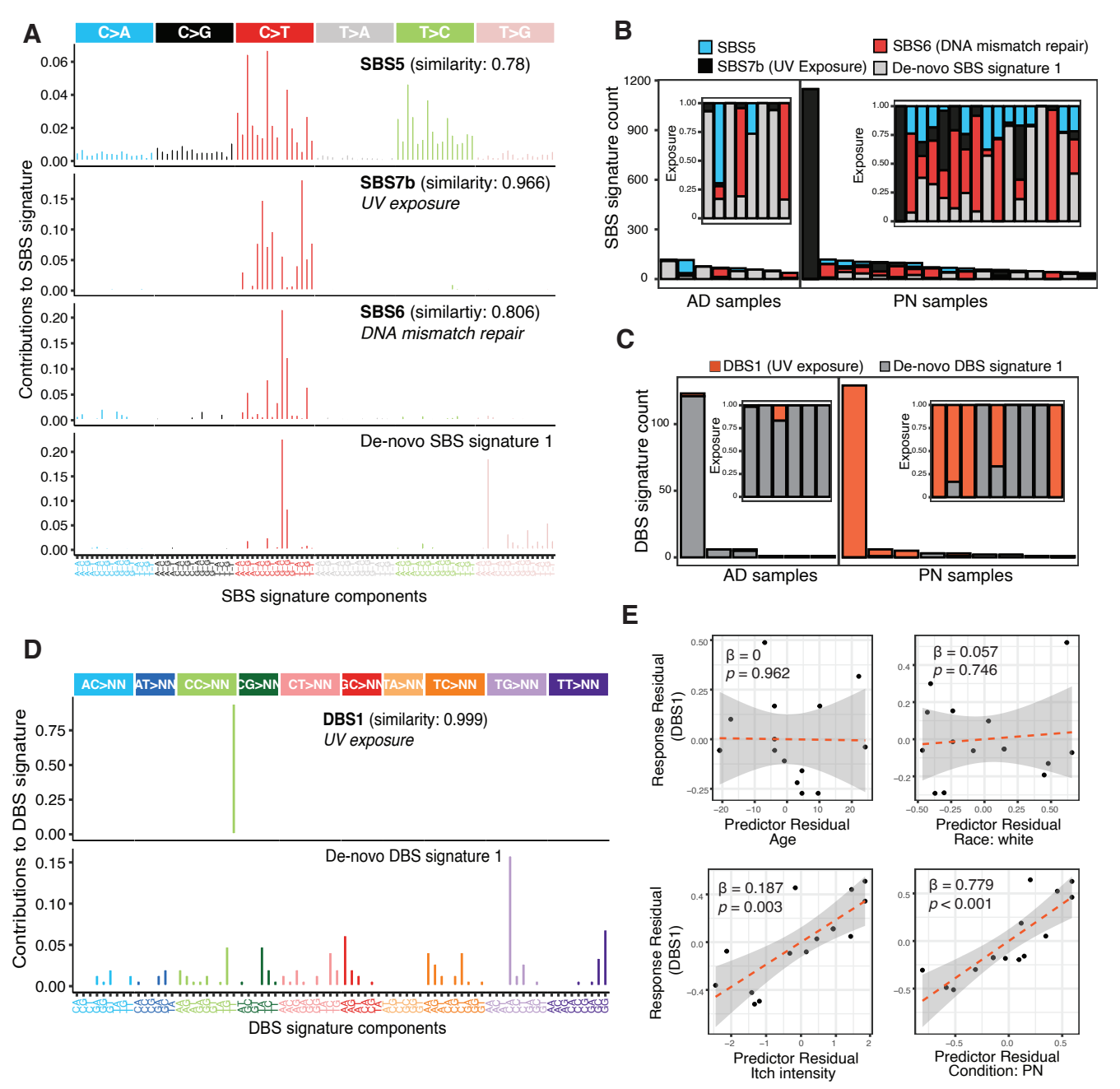
A
C>A
C>G
C>T
T>A
T>C
T>G
SBS5 (similarity: 0.78)
SBS7b (similarity: 0.966)
UV exposure
SBS6 (similartiy: 0.806)
DNA mismatch repair
De-novo SBS signature 1
Contributions to SBS signature
SBS signature components
B
SBS5
SBS6 (DNA mismatch repair)
SBS7b (UV Exposure)
De-novo SBS signature 1
SBS signature count
Exposure
AD samples
PN samples
C
DBS1 (UV exposure)
De-novo DBS signature 1
DBS signature count
AD samples
PN samples
D
AC>NN
AT>NN
CC>NN
CG>NN
CT>NN
GC>NN
TA>NN
TC>NN
TG>NN
TT>NN
DBS1 (similarity: 0.999)
UV exposure
De-novo DBS signature 1
Contributions to DBS signature
DBS signature components
E
β = 0
p = 0.962
Response Residual (DBS1)
Predictor Residual Age
β = 0.057
p = 0.746
Predictor Residual Race: white
β = 0.187
p = 0.003
Predictor Residual Itch intensity
β = 0.779
p < 0.001
Predictor Residual Condition: PN

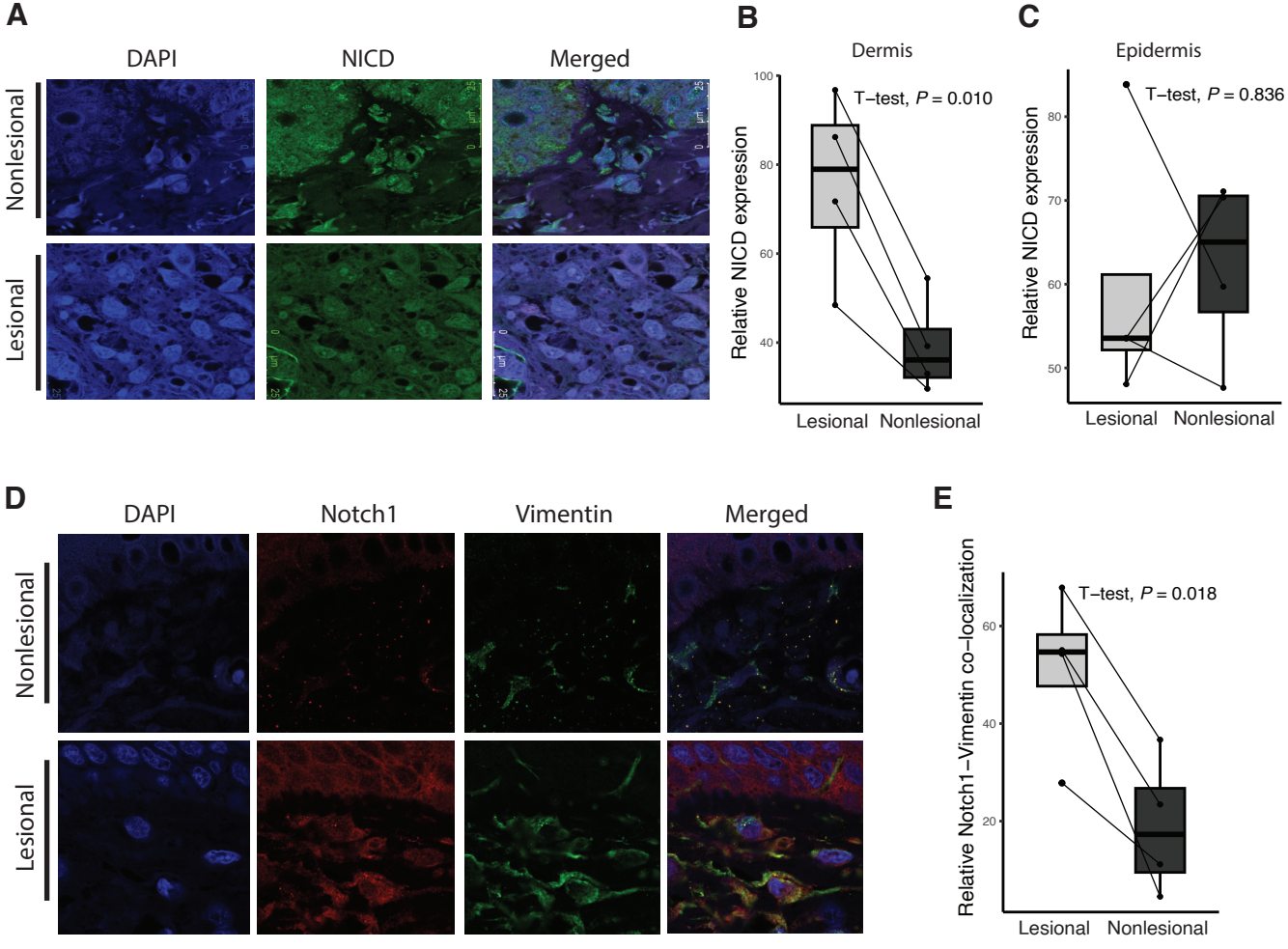
A
DAPI
NICD
Merged
Nonlesional
Lesional
B
Dermis
T–test, P = 0.010
Relative NICD expression
100
80
60
40
Lesional
Nonlesional
C
Epidermis
T–test, P = 0.836
Relative NICD expression
80
70
60
50
Lesional
Nonlesional
D
DAPI
Notch1
Vimentin
Merged
Nonlesional
Lesional
E
T–test, P = 0.018
Relative Notch1–Vimentin co–localization
60
40
20
Lesional
Nonlesional

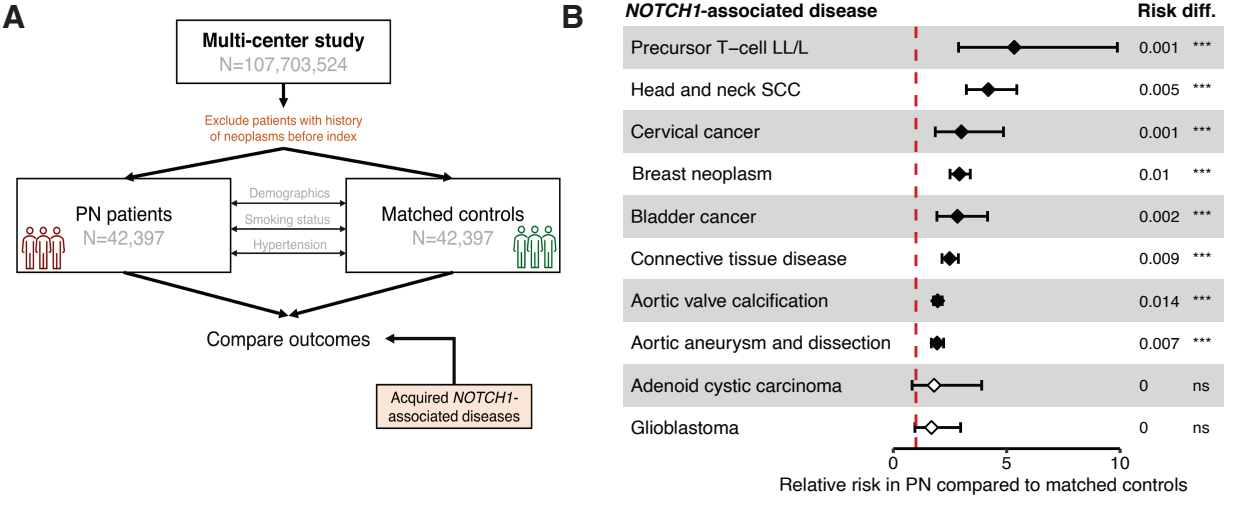
A
Multi-center study
N=107,703,524
Exclude patients with history of neoplasms before index
PN patients
N=42,397
Demographics
Smoking status
Hypertension
Matched controls
N=42,397
Compare outcomes
Acquired NOTCH1-associated diseases
B
NOTCH1-associated disease
Risk diff.
Precursor T–cell LL/L
0.001 ***
Head and neck SCC
0.005 ***
Cervical cancer
0.001 ***
Breast neoplasm
0.01 ***
Bladder cancer
0.002 ***
Connective tissue disease
0.009 ***
Aortic valve calcification
0.014 ***
Aortic aneurysm and dissection
0.007 ***
Adenoid cystic carcinoma
0 ns
Glioblastoma
0 ns
0
5
10
Relative risk in PN compared to matched controls